The Role of Network Architecture in Collagen Mechanics

K.A. Jansen[1,2], A. J. Licup[3], A. Sharma[3,4], R. Rens[3], F.C. MacKintosh[3,5,6,*], G.H. Koenderink[1,*]

[1]AMOLF, Biological Soft Matter group, Science Park 104, 1098 XG Amsterdam, The Netherlands. [2]UMC Utrecht, Department of Pathology, Universiteitsweg 100, Stratenum 2.118, 3584 CG Utrecht, The Netherlands. [3]Department of Physics and Astronomy, Vrije Universiteit, 1081 HV Amsterdam, The Netherlands. [4] Leibniz-Institut für Polymerforschung Dresden, 01069 Germany. [5] Departments of Chemical & Biomolecular Engineering, Chemistry, and Physics & Astronomy, Rice University, Houston, TX 77005, USA. [6] Center for Theoretical Biophysics, Rice University, Houston, TX 77030, USA

Abstract

Collagen forms fibrous networks that reinforce tissues and provide an extracellular matrix for cells. These networks exhibit remarkable strain-stiffening properties that tailor the mechanical functions of tissues and regulate cell behaviour. Recent models explain this nonlinear behavior as an intrinsic feature of disordered networks of stiff fibers. Here we experimentally validate this theoretical framework by measuring the elastic properties of collagen networks over a wide range of self-assembly conditions. We show that the model allows us to quantitatively relate both the linear and nonlinear elastic behavior of collagen networks to their underlying architecture. Specifically, we identify the local coordination number (or connectivity) $\langle z \rangle$ as a key architectural parameter that governs the elastic response of collagen. The network elastic response reveals that $\langle z \rangle$ decreases from 3.5 to 3 as the polymerization temperature is raised from 26 to 37°C while being weakly dependent on concentration. We furthermore infer a Youngs modulus of 1.1 MPa for the collagen fibrils from the linear modulus. Scanning electron microscopy confirms that $\langle z \rangle$ is between 3 and 4, but is unable to detect the subtle changes in $\langle z \rangle$ with polymerization conditions that rheology is sensitive to. Finally, we show that, consistent with the model, the initial stress-stiffening response of collagen networks is controlled by the negative normal stress that builds up under shear. Our work provides a predictive framework to facilitate future studies of the regulatory effect of extracellular matrix molecules on collagen mechanics. Moreover, our findings can aid mechanobiological studies of wound healing, fibrosis and cancer metastasis, which require collagen matrices with tunable mechanical properties.

1 Introduction

Collagens form a family of around 30 proteins that are crucial structural molecules in the human body (1). The most abundant family member is collagen type I, which forms fibrillar networks that shape and reinforce tissues such as skin, tendons, and bone. The structure of these networks is tailored towards diverse tissue-specific functions by auxiliary extracellular matrix molecules and by biochemical and mechanical activities of cells. Collagen in load-bearing tendons for instance forms thick fibers (200 nm) that are aligned along the tendon to optimize force transmission and tendon strength (2). In contrast, collagen in the cornea forms woven sheets of thin fibers ($\sim$30 nm) that provide strength combined with optical transparency (3). Collagen in interstitial tissue forms mostly isotropic networks, which provide mechanical strength combined with porosity to facilitate nutrient transport and cell migration (4).

Collagen structure and mechanics not only determine the function of the tissue as a whole, but also the functions of the cells that are resident in the tissue. Collagen fibers provide cells with topographical, biochemical and mechanical cues, which regulate cell proliferation, differentiation, migration, and apoptosis (5). The mechanobiological interplay between cells and the surrounding collagen extracellular matrix is essential to guide physiological processes such as wound healing and immune cell trafficking, but it can also trigger pathological processes. Abnormal stiffening of interstitial collagen networks for instance promotes cell invasion, which contributes to cancer, atherosclerosis, and chronic fibrosis.

0006-3495/08/09/2624/12 $2.00 doi: .....

The importance of collagen mechanics in biology has triggered a long history of research on the relation between collagen structure and mechanics. It is long known that collagenous tissues exhibit a distinctive non-linear elasticity characterized by strain-induced stiffening (6). This mechanical design allows tissues such as skin and arteries to be soft at low strain yet stiff at high strain, ensuring mechanical stability under large loads (7). However, the complex architecture of collagenous tissues, which comprises multiple scales, has made it difficult to pinpoint the structural basis of the strain-stiffening response. Tissues contain networks of fibril bundles, which in turn contain hundreds of molecules per cross-section packed in an axially ordered lattice (8). *In situ* X-ray scattering studies suggest that multiple mechanisms operating at different length scales contribute to the overall mechanical response at the tissue level (9).

The challenge to elucidate the origin of the nonlinear elasticity of collagenous tissues has motivated intensive efforts to study simplified model systems reconstituted from purified collagen. This development was further fuelled by the rapid growth of the interdisciplinary field of mechanobiology, where reconstituted collagen networks are popular as tissue equivalents in basic studies of the biology of tissues, wound healing, immunity, and cancer and in more applied studies relating to regenerative medicine (10, 11). Conveniently, the self-assembly of collagen into fibrillar networks is encoded in the collagen molecule itself. Under physiologically relevant buffer conditions, collagen spontaneously assembles into axially ordered fibrils, which branch and crosslink to form a three-dimensional network (1). The diameter of the fibrils can be tuned from tens of nanometers to several microns by changing environmental conditions such as the solution pH (12–14) and polymerization temperature (15–17).

It is well-established that reconstituted collagen networks stiffen in a similar manner as whole tissues when they are subjected to a mechanical stretch or shear (12, 18–21). However, even in this more simplified context of reconstituted networks, theoretical modelling remains challenging due to the range of scales. The most detailed models, based on full-atom simulations, are limited to single collagen molecules and microfibrils and require coarse-graining approaches to reach up to the fibril level (22, 23). Recent models aimed to describe collagen at the network level therefore usually treat the fibrils as homogeneous elastic beams (20, 24, 25). These models predict that the elasticity of collagen networks is primarily governed by the local connectivity z, meaning the number of fibers that meet at each network junction. Since collagen fibers are connected by a combination of branch points ($z = 3$) and crosslinks ($z = 4$), z is on average between 3 and 4 (20, 25, 26). In networks of springs that possess only stretching energy, such a low connectivity is insufficient for mechanical stability in 3D, where the isostatic limit is $z = 6$ (27). Fibrous networks such as collagen networks, however, are stabilized by the high bending rigidity of the fibers (20, 28).

Recent experiments on reconstituted collagen I networks confirmed some of the predictions of these fiber-based network models (20, 25, 29). However, the general validity of this model for collagen networks reconstituted over a wider range of self-assembly conditions remains untested. Consequently, a clear consensus on the physical basis of the elasticity of collagen networks is still lacking. Random fiber models generally predict that the network stiffness at small strain should go up with collagen concentration as a power law with an exponent of 2 (30, 31). But experimentally, a wide range of exponents between 1 and 3 has been observed (18, 19, 32–36). It was recently suggested that this range can be accounted for by a systematic variation in local architecture with concentration (25), although this hypothesis has yet to be tested experimentally. Moreover, this model also made another interesting prediction that still lacks experimental verification: strain-stiffening is predicted to be coupled to a build-up of a negative (contractile) normal stress under shear (20). While there have been reports of negative normal stresses in filamentous networks including collagen (37, 38), which is opposite to the response of most elastic solids and polymer hydrogels (37, 39), the relationship of negative normal stress to strain-stiffening has not been quantitatively demonstrated experimentally.

The goal of this work is to quantitatively decipher the relation between the mechanics and underlying architecture of fibrillar collagen networks reconstituted from purified collagen I. We show that a model of disordered fiber networks provides a self-consistent framework to quantitatively explain both the linear and nonlinear elastic properties of collagen networks over a wide range of concentrations (0.5-5 mg/ml) and assembly temperatures (between 26 and 37°C). We probed the elastic properties of the networks by macroscopic shear rheometry and characterized the network architecture by combining light scattering, scanning electron microscopy and confocal reflectance microscopy. We find that as the stress applied to a collagen network is increased, the network stiffens in two stages. In the first regime, network stiffening is coupled to the simultaneous build-up of self-generated negative normal stress, as predicted for bending-dominated networks (20). In the second stage, stiffening is caused by a mechanical phase transition to a stretch-dominated response above a critical strain value γ_c (25). Interestingly, our data suggest that the elastic properties of collagen networks are sensitive to subtle changes in network architecture with changing collagen concentration and polymerization temperature.

2 Materials and Methods

A detailed description of the experimental and computational methods is provided in the online supplementary data. Experiments were performed on collagen networks reconstituted from rat tail collagen type I in a buffer that is compatible with *in vitro* cell culture (DMEM cell culture medium, 1% FBS, 50 mM HEPES, 1.5 mg/ml sodium bicarbonate and 0.1% antibiotics, pH 7.3−7.4). Networks were polymerized at temperatures between 22 and 37°C and at collagen concentration between 0.7 and 5 mg/ml. Rheology was performed with a stress-controlled rheometer (Physica MCR 501, Anton Paar, Graz, Austria) using a cone-plate geometry with 40 mm diameter and 1° cone angle. The networks were polymerized *in situ* for 6 hours before rheological testing. Turbidity measurements were performed using a Cary300 UV-Vis spectrophotometer (Agilent Technologies, Amstelveen, Netherlands) on networks prepared in plastic cuvettes (UV-Cuvette micro, Plastibrand, Germany) for 6 hours or overnight. Rheological and turbidity data shown are averages ± standard deviation for a minimum of 3 independently prepared samples. Collagen networks were imaged by confocal reflectance microscopy with an inverted Eclipse Ti microscope (Nikon), using an 488 Ar laser (Melles Griot, Albuquerque, NM) for illumination and a 100x N.A. 1.49 or 40x N.A. 1.30 objective. Fixed and dried networks of 4 mg/ml collagen coated with Au/Pd were imaged by scanning electron microscopy (Verios 460, FEI Company, Eindhoven, the Netherlands). Computational modelling of collagen networks was performed by representing the networks as 2D disordered triangular lattices, described in detail elsewhere (20, 25, 40). These lattices have a spacing l_c and dimensions WxW, where $W = 50l_c$. We enforce local 4-fold connectivity by a phantomization procedure, where a binary cross-link is formed between two randomly selected fibers at each vertex while treating the third fiber as a phantom that does not interact with the other two fibers. Next we reduce $\langle z \rangle$ to a value between 3 and 4 by bond dilution, which involves random removal of segments with a probability q. This procedure reduces the average fiber length to $L = l_c/q$. Thus, the networks are, by construction, sub-isostatic and floppy in the absence of bending interactions. Each filament is assigned a stretching modulus, μ_s, and a bending modulus, κ. The lattices are subjected to a simple shear strain, γ, and allowed to relax by minimization of the total elastic energy per unit volume, H, which is calculated according to a discrete form of the extensible wormlike chain Hamiltonian. The stress follows from the minimum energy as: $\sigma = dH/d\gamma$, while the differential elastic shear modulus follows as: $K = d^2H/d\gamma^2$. Stress and stiffness are measured in units of μ/l_c^{d-1}, where d is the dimensionality.

3 Results

3.1 Collagen network architecture depends on polymerization conditions

Our goal was to quantitatively decipher the relation between the mechanics and underlying architecture of fibrillar collagen networks reconstituted from purified collagen I. To tune the structure of the networks, we varied the polymerization temperature, motivated by prior work demonstrating that temperature strongly influences the architecture of collagen networks (15, 41, 42). To visualize the network structure, we use confocal reflectance microscopy (CRM), which is an ideal technique for non-invasive and label-free imaging of collagen (43). We observe striking changes in network structure when we polymerize 4 mg/ml collagen at different temperatures between 22 and 37°C, as shown in the top row of images in Fig. 1 (see Fig. S1 for the full range of temperatures and a broader range of magnifications). The networks are dense, isotropic, and uniform at temperatures of 30°C and above. In contrast, they appear more heterogeneous and open at lower temperatures, especially at 22°C, where we observe fan-shaped bundles of collagen fibrils. Similar fan-shaped bundles were observed previously at polymerization temperatures between 4 and 27°C (15, 41, 42) and were proposed to arise from the kinetic arrest of growing fibrils during network formation (42).

To obtain more high-resolution information regarding the network structure, we supplement CRM with Scanning Electron Microscopy (SEM) of dehydrated networks. The fan-shaped bundles at 22°C are also visible in SEM images, where they are seen to be bundles of fibrils that splay out at one end (Fig. 1, two bottom rows). Networks formed at 26°C also display bundles in SEM images, but their width is more uniform and the network microstructure appears more uniform than at 22°C. As the temperature is raised further, the networks remain homogeneous and become progressively less bundled. At 37°C the network looks homogeneous at all inspected length scales and bundling is minimal. To quantify the change in diameter of the fibers (i.e. fibril bundles) with temperature, we measured the cross-sectional width of at least 250 randomly sampled fibers per condition in SEM images recorded at magnifications between 10,000 and 50,000 for three independently prepared samples. We did not attempt to perform this analysis for SEM images of networks prepared at 22°C due to the open fan-shape of the collagen fibers of these networks. As shown in Fig. 2A, the average fiber diameter is around 150 nm at temperatures of 26 and 30°C (with a large spread at 26°C), while it is around 70 nm at both 34 and 37°C. We note that these values are expected to be different from the actual diameters of the fibers in their native, hydrated state. On the one hand, fiber shrinkage is expected

due to the solvent removal procedure required to prepare samples for electron microscopy, while on the other hand some thickening is expected due to the deposition of a metal coating that is required for imaging.

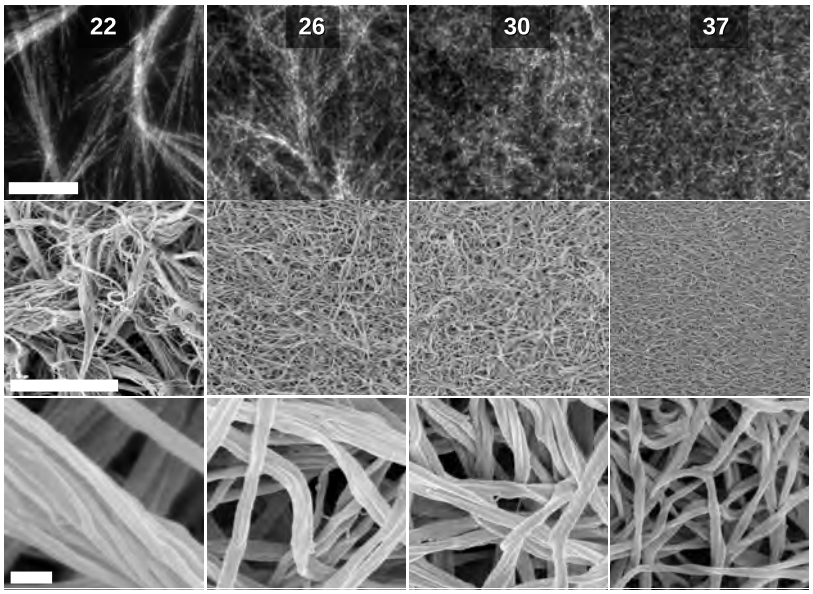

Figure 1: Temperature dependence of the microstructure of 4 mg/ml collagen networks. The temperature is indicated above each column in units of °C). *(row 1)* Confocal reflection images (row 1), showing an open network of 'fan-shaped' fibril bundles at 22 °C and more homogeneous and progressively denser networks with increasing temperature. Scanning Electron Microscopy (SEM) images at two different magnifications (rows 2 and 3). The scale bars denote 20 μm (row 1 and 2) and 200 nm (row 3). See Figure S1 in the supplementary information (SI) for additional data.

For comparison, we therefore also probed the fiber diameter by light scattering, a technique that is noninvasive and does not require dehydration (44). The basic idea is that the wavelength dependence of the turbidity of a fibrous gel, $\tau(\lambda)$, encodes information on the average diameter d and mass-length ratio μ of the fibers. Theoretical models for light scattering from random fiber networks (assumed to be monodisperse in diameter) predict that $\tau\lambda^5$ should increase linearly with λ^2 with a slope which depends on μ and an intercept dependent on μ and d (for details see Methods section in the SI). We indeed find approximately linear dependencies for collagen networks formed at temperatures between 26 and 37°C, consistent with the uniform microstructure seen in CRM and SEM images (Fig. S2). By contrast, we find a strongly nonlinear dependence for networks formed at 22°C, indicating that light scattering is sensitive to the structural heterogeneities in these networks. The μ and d values obtained at 22°C (by fitting the data for wavelengths between 650 and 890 nm) should therefore be regarded as approximate.

The diameters obtained by light scattering are nearly twofold higher than the values obtained from SEM images, indicating that the dehydration procedure needed to prepare SEM samples induces fiber shrinkage (see Fig. 2A). But the trend as a function of temperature is similar as observed by SEM: fibers formed at 22°C are thickest with an average diameter of 300 nm, fibers formed at 26 and 30°C have comparable average diameters of about 200 nm, while fibers formed at 34 and 37°C have smaller diameters of around 150 nm. The average mass length ratio of the fibers also decreases with increasing polymerization temperature (see Fig. 2B). From the change in μ, we can estimate the corresponding change in average mesh size, $\xi = (1/\rho_l)^{0.5}$, where $\rho_l = c_p/\mu$ is the total length of collagen fibers per unit volume (in m^{-2}) and c_p is the collagen concentration (in mg/ml). At 4 mg/ml collagen we expect a 2-fold reduction in ξ, from 3.3 to 1.6 μm, as the polymerization temperature is raised from 26 to 37°C, a trend that is qualitatively consistent with the CRM images. At each polymerization temperature, we find that both μ and d decrease with increasing collagen concentration (see Fig. 2B and Fig. S2B).

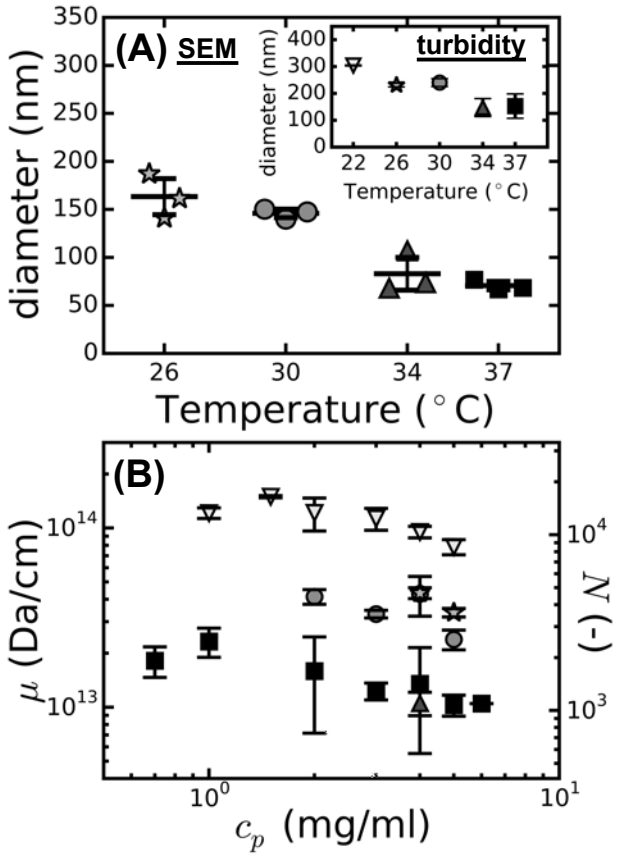

Figure 2: Comparison of fibril diameter measurements by electron microscopy on dried samples and turbidity measurements on hydrated samples. (A) Average fiber diameters for 4 mg/ml collagen networks polymerized at different temperatures determined from SEM images (main graph) and turbidimetry (inset). (B) Concentration dependence of the mass-length ratio obtained from turbidimetry for collagen networks formed at temperatures of 22 (triangles down), 26 (stars), 30 (circles), 34 (triangles up) and 37°C (squares). The left y-axis corresponds to the mass-length ratio μ, while the right y-axis shows the corresponding number of monomers per fibril cross-section, N (see Eq. (3) in the SI). Turbidity data are averages $\pm$ standard deviation for 3 samples per condition. SEM data are averages $\pm$ standard deviation of 3 samples per condiation, where at least 250 fibrils were analysed.

3.2 Collagen mechanics depend on polymerization conditions

3.2.1 Strain-stiffening behaviour of collagen networks

To test how the changes in network structure identified by microscopy and turbidimetry influence collagen mechanics, we first investigated the nonlinear elastic response of the collagen networks. Specifically, we probed the differential modulus, $K^* = \delta\sigma/\delta\gamma$, by subjecting the network to a stepwise increasing prestress, σ, while superposing small amplitude stress oscillations. We find that with increasing strain, the elastic modulus, K', strongly increases (Fig. 3A) until a maximum strainof 20-50% is reached, where the networks fail (Fig. S3 in the SI). We will refer to this strain as the failure point but we note that it is unclear whether failure is due to internal network rupture or detachment from the rheometer plates. The final stiffness just before network rupture is typically one order of magnitude higher than the linear modulus, consistent with prior reports (19, 34). The strain-stiffening response is reversible for all networks formed between 26 and 37°C, with little hysteresis between forward and backward sweeps and reproducible strain-stiffening in consecutive runs (Fig. S4 in the SI). By contrast, networks formed at 22°C show significant hysteresis and progressive softening in repeated stress ramps.

A closer inspection of the strain-stiffening curves reveals two distinct stiffening regimes demarcated by two distinct characteristic strain values. The first characteristic strain, which we denote as γ_0, corresponds to the end of the linear elastic regime and onset for strain-stiffening (red symbols in Fig. 3A). While γ_0 is difficult to identify unambiguously from the

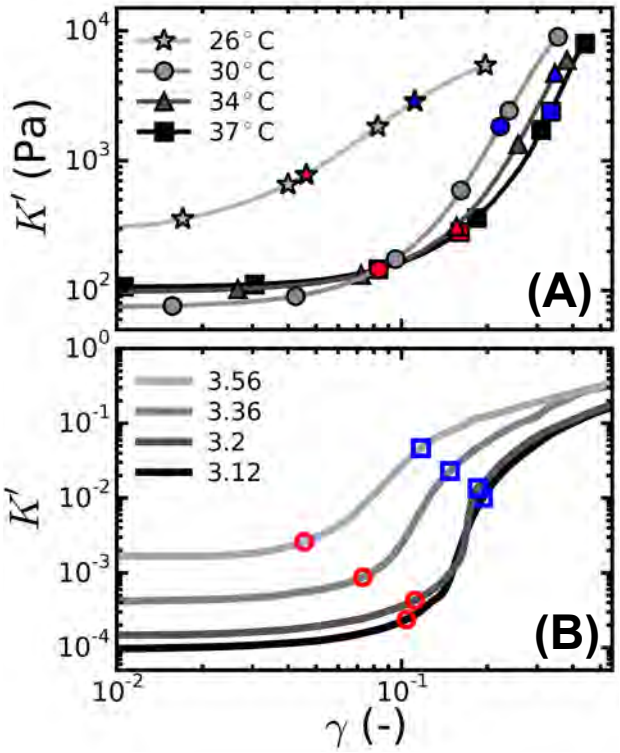

Figure 3: Comparison of the strain-stiffening response of collagen networks with simulations of disordered 2D fibrous networks. The differential elastic modulus K' is plotted as a function of the applied shear strain, γ. Red symbols denote the onset strain where stiffening sets in (γ_0, see Fig. S5). Blue symbols denote the critical strain for the transition to stretch-dominated elasticity, (γ_c, see Fig. S6). Data shown are representative examples measured on single networks. Symbols are shown for clarification only, every 5^{th} datapoint is shown. (A) Measurements for 4 mg/ml collagen networks polymerized at temperatures between 26 and 37°C (see legend). (B) Simulation data for 2D fibrous networks with a fixed dimensionless rigidity, $\widetilde{\kappa} = 10^{-4}$, and varying average connectivity $\langle z \rangle$ (see legend).

strain-stiffening curves, it can be clearly identified when we plot $K'(\sigma)/\sigma$ as a function of σ (Fig. S5 in the SI). The second characteristic strain, which we denote as γ_c (blue symbols in Fig. 3A), is closer to the failure point. This characteristic strain is well-defined as the inflection point of the strain-stiffening curves (see Fig. S6 in the SI). We see that both γ_0 and γ_c increase with the polymerization temperature (Fig. 4A).

Can we quantitatively explain these changes in the strain dependent elasticity of the collagen networks in terms of their architecture? To answer this, we employ a computational model that represents a collagen network as a disordered network of elastic fibers, based on an initial two-dimensional (2D) triangular lattice (20, 25, 40). We use 2D simulations, because these are much less computationally intensive than 3D simulations, which allows us to scan a wider parameter space with larger systems that are less sensitive to finite-size effects. Prior work has shown good consistency of 2D and 3D simulations of such models, provided that the average coordination number $\langle z \rangle$ is well below the 2D isostatic point of 4 (28, 45). This model assumes that thermal fluctuations are negligible, an assumption that is amply justified by fluctuation analysis (46) and various mechanical measurements (47–53) on single collagen fibers. Each filament is assigned a stretching modulus, μ_s, and a bending modulus, κ. These two parameters define a dimensionless measure of the relative bend-stretch stiffness: $\widetilde{\kappa} = \kappa/\mu_s l_c^2$. We note that our model networks are disordered, even though they are based on an initial lattice structure: both the connectivity and fiber length, for instance, vary from point to point within the network.

Consistent with the experimental observations, the simulations reveal a two-stage strain-stiffening response with an onset strain γ_0 (red circles) and an inflection at a critical strain γ_c (blue squares), as shown in Fig. 3B (see also Fig. S5 and S6 in the SI). As we progressively increase $\langle z \rangle$ from 3.12 (black line) to 3.56 (lightest gray line), we see that G_0 increases, while γ_0 and γ_c decrease. These shifts are qualitatively consistent with the shifts we observe in collagen networks as we reduce the

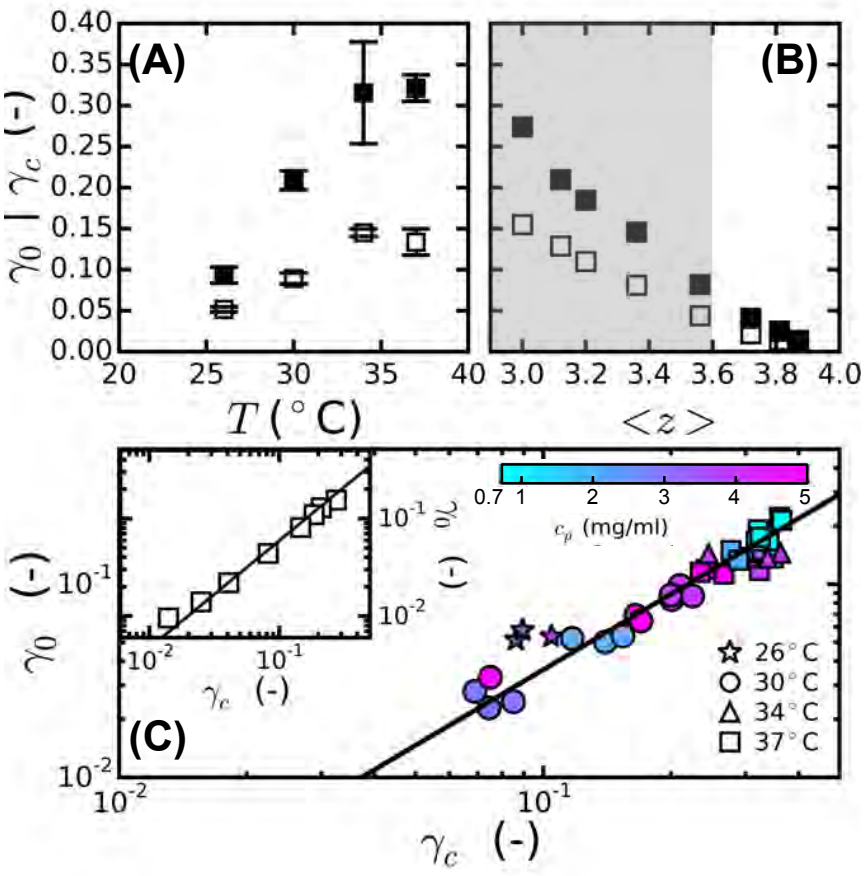

Figure 4: Comparison of the onset strain and the critical strain that characterize the strain-stiffening response of collagen networks with predictions for 2D fibrous networks. (A) Measurements of γ_0 (open symbols) and γ_c (closed symbols) for 4 mg/ml collagen networks. Data points are averages $\pm$ standard deviation for 3 samples per condition. (B) Corresponding simulation results showing the $\langle z \rangle$-dependence of γ_0 and γ_c for 2D networks with $\widetilde{\kappa} = 10^{-4}$, a value that is representative of collagen networks at concentrations in the range of several mg/ml (25). The $\langle z \rangle$-range relevant to the experiments is highlighted in grey. (C) The experiments (main plot) are in excellent agreement with the simulations (inset), which predict a power-law dependence of γ_0 on γ_c with an exponent given by $\phi - f$. The lines have slopes of 1.3 (main) and 1.1 (inset), based on predicted values of ϕ and f in Table S2 in the SI. Data points represent individual measurements (at least 3 per condition) obtained at collagen concentrations c_p between 0.7 and 5 mg/ml and polymerization temperatures between 26 and 37°C (see legends).

polymerization temperature. We therefore hypothesize that the temperature dependence of the nonlinear elasticity of collagen networks may be caused by a change in the network connectivity.

To test this hypothesis, we directly compare the γ_0 and γ_c values determined in experiments and in simulations (Fig. 4A,B). In the experimentally relevant $\langle z \rangle$ range (between 3 and 3.5), the strain values in experiments and simulations are in close agreement. Using the simulations as a reference point, we can infer from the correspondence with the experiments that the shift to larger γ_0 values as the polymerization temperature is raised from 26°C to 37°C is consistent with a decrease in $\langle z \rangle$ from about 3.5 to 3 (see Fig. 5B and Table S1). We note that all concentrations tested at 30°C show higher $\langle z \rangle$ values compared to the 37°C case (Fig. 5A). At 37°C, $\langle z \rangle$ is below 3 at the lowest concentrations of 0.7 and 1 mg/ml, while it is close to 3 for collagen concentrations between 2 and 4 mg/ml, and increases to almost 3.2 at 5 mg/ml (see Fig. 5A (black squares) and Table S1).

The values of $\langle z \rangle$ we infer from the nonlinear rheology predicted by our model are qualitatively consistent with the SEM images of 4 mg/ml networks prepared at different temperatures. In these images, we observe predominantly 3-fold branches

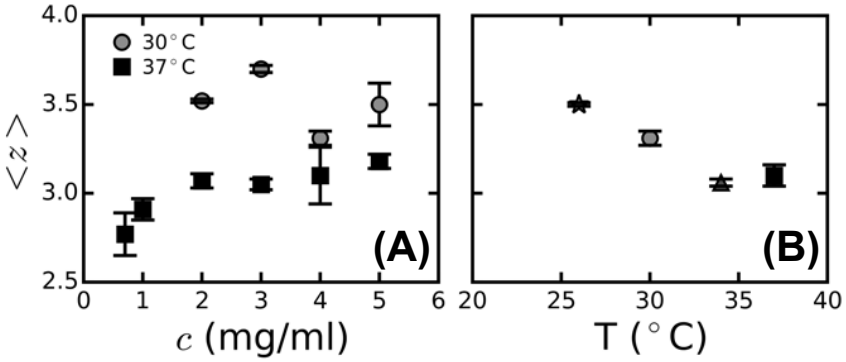

Figure 5: Average connectivity $\langle z \rangle$ of collagen networks inferred from rheology data by calibrating measurements of γ_0 with simulation data for 2D fibrous networks (see Fig. 4A,B). (A) Concentration dependence of $\langle z \rangle$ at a polymerization temperature of 37°C (black squares) and 30°C (gray circles). (B) Temperature dependence of $\langle z \rangle$ at a collagen concentration of 4 mg/ml. Data points are averages $\pm$ standard deviation for 3 samples per condition. The data are also tabulated in Table S1.

and 4-fold junctions (see Fig. S7). The images do not reveal a significant dependence of $\langle z \rangle$ on polymerization temperature. It is difficult, however, to measure $\langle z \rangle$ reliably from imaging alone. The problem is that imaging cannot unambiguously distinguish whether an apparent junction of two fibers in a static image is a crosslinked pair or just an entangled pair, and it is furthermore difficult to determine whether the fiber ends are crosslinked to other fibers or dangling. The SEM images show that fibers emerging from branch points often have unequal diameters. In the context of our model, such variation in fiber diameter and possible unequal distribution of material at branch ($z = 3$) or crossing ($z = 4$) points represents a kind of (quenched) disorder. We do not include variation in the fiber diameter in the present model. In previous theoretical work where we tested the effect of inhomogeneous fiber diameter in branched networks, we did not find qualitative differences in the network rheology (54).

As a further test of our hypothesis that the fibrous network model can explain the nonlinear elasticity of collagen networks, we check for the correlation between γ_0 and γ_c. The simulations predict that γ_0 should increase with γ_c according to $\gamma_0 \sim \gamma_c^{(\phi - f)}$ (inset of Fig. 4C). The physical basis of this relationship is that collagen networks undergo a strain-controlled transition from an elastic regime governed by fiber bending to an elastic regime governed by fiber stretching when the strain reaches γ_c (25, 40). Simulations predict that this phase transition is governed by two critical exponents, ϕ and f, which are nearly identical for 2D and 3D networks (25, 29). Using values for these exponents determined in simulations of 2D lattices for varying $\langle z \rangle$ (see Table S2), we find quantitative agreement of the measured values of γ_0 and γ_c with the theory (solid line) for all polymerization temperatures (color-coded symbols) without any adjustable parameters (Fig. 4C). This remarkable agreement provides additional strong evidence that collagen networks over a range of concentrations (0.7 -5 mg/ml) and polymerization temperatures (26-37°C) can be modelled as athermal random networks of elastic fibers. Our findings furthermore suggest that the nonlinear elasticity of collagen networks is sensitive to small changes in average network connectivity that are not readily apparent from microscopy images.

3.2.2 Low-strain mechanics of collagen

We have shown that a coarse-grained model that describes collagen networks as disordered networks of elastic fibers can successfully explain the nonlinear elastic response of collagen networks over a wide range of collagen concentrations and polymerization temperatures. An additional critical test of the model is whether it can also predict the magnitude of the linear elastic modulus at small strains below the onset of the nonlinear regime. We find that the linear modulus of the collagen networks, as quantified by $G_0 = G'(0.5\text{Hz})$, shows a non-monotonic dependence on polymerization temperature (solid symbols in Figure 6A): At a concentration of 4 mg/ml, the collagen gels are stiffest at 22 and 26°C, while they are softest between 30 and 37°C. To test whether we can relate this temperature dependence to the changes in network structure, we compare the measured moduli to theoretical predictions, according to which G_0 can be written as:

$$G_0 = F(z) E \varphi^2, \tag{1}$$

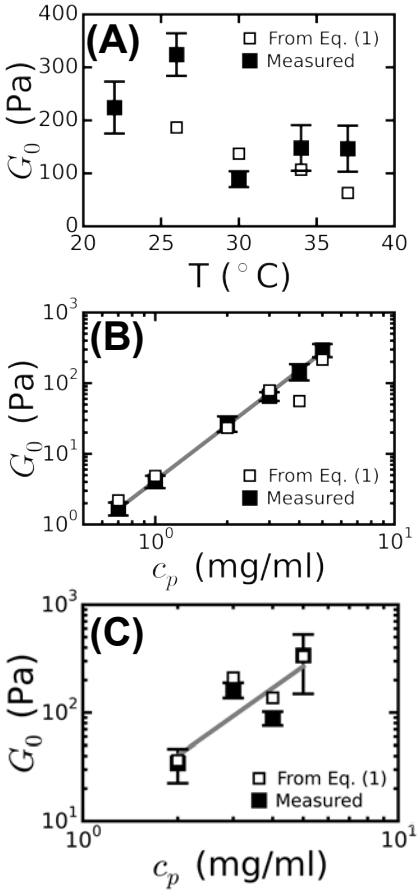

Figure 6: Comparison between measurements of the linear elastic modulus of collagen gels (closed symbols) and theoretical predictions for 3D fibrous networks (open symbols). The theoretical values are calculated according to Eq. 1, which takes as input $\langle z \rangle$ as inferred from the nonlinear rheology (Fig. 5 and Table S1), the fiber mass-length as measured by turbidimetry (Fig. 2), and the fiber Young's modulus E as the sole fitting parameter. (A) Temperature dependence of $G_0 = G'(0.5\text{Hz})$ for 4 mg/ml collagen gels. (B) Concentration dependence of G_0 for networks polymerized at 37°C and (C) 30°C. The lines in panels B and C denote power-law fits with exponents of 2.6 and 2.1, respectively. Data points are averages $\pm$ standard deviation for 3 samples per condition. The data are also tabulated in Table S1.

where $F(z) \simeq \frac{A}{z}\frac{\sqrt{2}}{12\pi}\left(\frac{L}{l_c}\right)^2$ and L is the average fiber length. The network geometry as characterized by $\langle z \rangle$ enters Eq. 1 only through $F(z)$. In case $\langle z \rangle$ (and therefore $F(z)$) is independent of collagen concentration, the linear modulus should scale quadratically with the fiber volume fraction φ, consistent with prior athermal network models (30, 31). Any deviation from a quadratic scaling therefore signifies a concentration dependence of $\langle z \rangle$. We observe a clear deviation from this scaling for collagen networks polymerized at 37°C, where the power law exponent is 2.6 (indicated by the line in Fig. 6B). This indicates an increase of $\langle z \rangle$ with concentration, consistent with the conclusions we draw from the concentration dependence of γ_0 (see Fig. 5A). For networks polymerized at 30°C, the concentration dependence is closer to quadratic, with a best-fit exponent of 2.1.

To test this apparent self-consistent agreement between the linear and nonlinear elastic behaviour more closely, we compare for each experimental condition the measured G_0 with the theoretically expected modulus, calculated from Eq. 1 using as input the $\langle z \rangle$ values inferred from the onset strain (see Table S1). The sole unknown parameter used for fitting is the fiber Young's modulus E. As shown in Fig. 6, the theory captures both the temperature dependence of G_0 at fixed collagen concentration (panel A) and the concentration dependence of G_0 at 37°C (panel B) and 34°C (panel C) rather well when we assume $E = 1.1$ MPa throughout. Note that we excluded data obtained for networks polymerized at 22°C from this analysis because

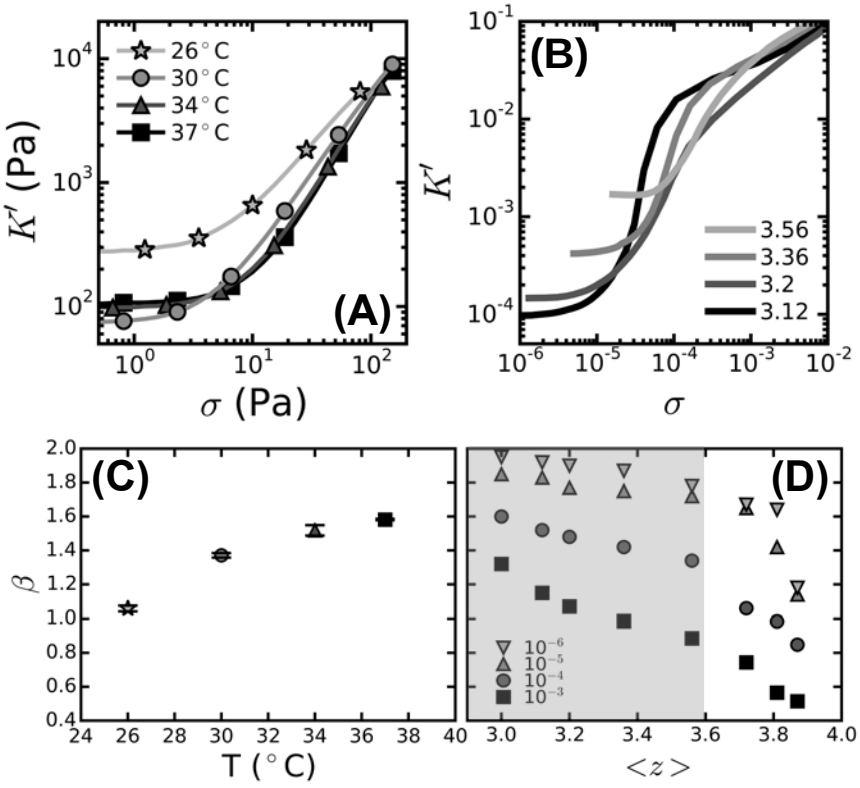

Figure 7: Comparison of the stress-stiffening response of collagen networks with predictions for 2D fibrous networks. (A) Example stiffening curves for 4 mg/ml collagen gels polymerized at different temperatures (see legend). The data shown are representative measurements on single networks. (B) Example stiffening curves for 2D fibrous networks with different connectivities $\langle z \rangle$ (see legend) and $\widetilde{\kappa}$ =10^{-4} (B). (C) The stiffening exponent β, defined as the maximum slope of the stress-stiffening curves in the nonlinear regime, increases with temperature. Data points are averages $\pm$ standard deviation for 3 samples per condition. (D) The simulations show that β depends on both $\widetilde{\kappa}$ and $\langle z \rangle$. The highlighted region depicts the $\langle z \rangle$-range relevant to the experiments.

these networks were too heterogeneous to extract reliable values for the fiber mass-length-ratio by light scattering (see Fig. S2A) and also because the nonlinear rheology data show hysteresis (Fig. S4A).

The agreement between theory and experiment is less good in Fig. 6A than it is in Fig. 6B and C. We suspect that this is due to inaccuracies in the fiber mass length ratio μ, which is required as input to calculate G_0 (see Eq. 8 in the Supporting Information). We obtain μ from turbidimetry, which requires a theoretical model with several simplifying assumptions, including diameter monodispersity. We suspect that μ is more accurate for the more homogeneous networks formed at 30 and 37°C (data in Fig. 6B and C) than for the somewhat bundled networks formed at lower temperatures (data in Fig. 6A). Note that the fact that we use experimental input for μ and that μ apparently changes with polymerization temperature and collagen concentration also explains the non-monotonicity of the predicted dependencies of G_0 in Fig. 6. Altogether, we think that the overall good agreement of theory and experiment over a range of collagen concentrations and assembly temperatures and for a reasonable value of E (see Discussion) provides convincing evidence that collagen networks over a wide range of assembly conditions can indeed be modelled as random networks of elastic fibers.

3.2.3 Stress-stiffening behavior of collagen networks

In addition to considering the dependence of collagen elasticity on strain, it is also instructive to consider its dependence on the applied shear stress. As shown in Fig. 7A, K' increases as a power law in σ with a stiffening exponent β that increases as the polymerization temperature is raised. As shown in Fig. 7C, β increases from a value close to 1 at 26°C to 1.6 at 37°C. When we perform a set of simulations on 2D fibrous networks for connectivities $\langle z \rangle$ between 3.12 and 3.56 and a fixed $\widetilde{\kappa}$ of

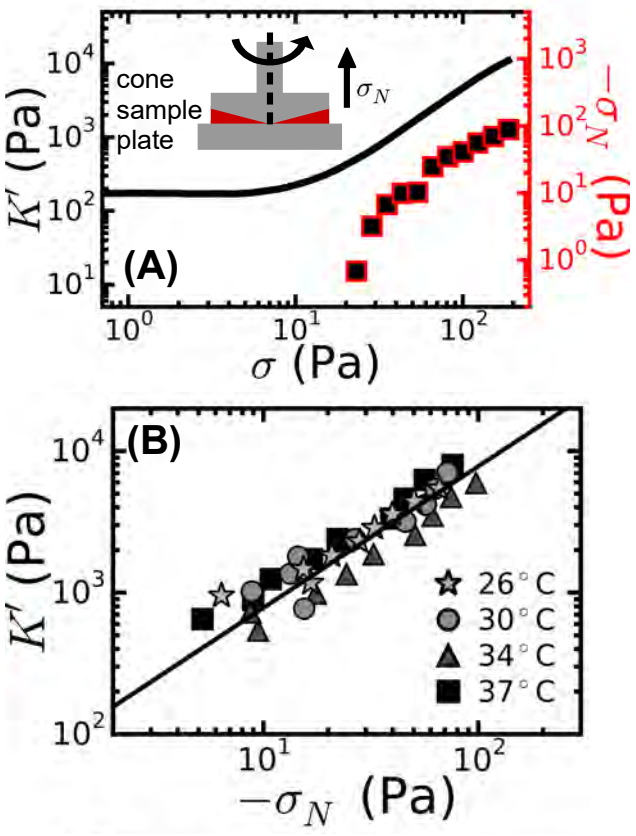

Figure 8: Sheared collagen networks develop a negative normal stress whose magnitude is linearly related to the nonlinear elastic modulus. (A) Example measurement showing simultaneous stiffening (black line, left y-axis) and the development of a negative normal stress (σ_N, right y-axis) for a 4 mg/ml collagen network at 37°C. The inset shows a schematic side view of the cone-plate measurement geometry and indicates the directions of the shear stress σ and normal stress σ_N. (B) K increases linearly with $-\sigma_N$ for 4 mg/ml collagen gels polymerized at temperatures between 26 and 37°C (see legend). One representative measurement per temperature condition is plotted. The solid line shows the expected power law dependence with exponent 1.

10^{-4}, we find that β strongly depends on $\langle z \rangle$ (Fig. 7B). By contrast, β changes little when $\widetilde{\kappa}$ is varied in the relevant $\langle z \rangle$ range (Fig. S8B in the SI). Consistent with this predicton, we find only a weak concentration dependence for β in the experiments (Fig. S8A).

As summarized in Fig. 7D, the simulations predict that β should decrease with increasing $\langle z \rangle$. The predicted values for $\beta \sim 1.0 - 1.6$ in the relevant $\langle z \rangle$ range between 3 and 3.5 are consistent with the experimentally observed range of β-values. By comparing the observed temperature dependence and predicted $\langle z \rangle$-dependence of β, we infer an apparent decrease of $\langle z \rangle$ from 3.7 to 3 as we raise the polymerization temperature from 26 to 37°C. This conclusion is entirely in line with the apparent decrease of $\langle z \rangle$ we inferred from the temperature dependence of γ_0 and γ_c. We once again conclude that the nonlinear elasticity of collagen networks appears to be sensitive to small changes in network connectivity.

3.3 Normal stress stabilizes collagen networks

We have shown that both the linear and nonlinear elasticity of collagen networks are in close agreement with theoretical predictions for networks of elastic fibers. As a final critical test of the model, we consider the normal stress that the networks develop when they are sheared. It is well-established that fibrous network develop a negative (contractile) normal stress when they are sheared between two plates with a fixed gap (37). Several analytical models and simulations for fibrous networks predict that stress-stiffening should be accompanied by an increase of the magnitude of this normal stress (37, 55, 56).

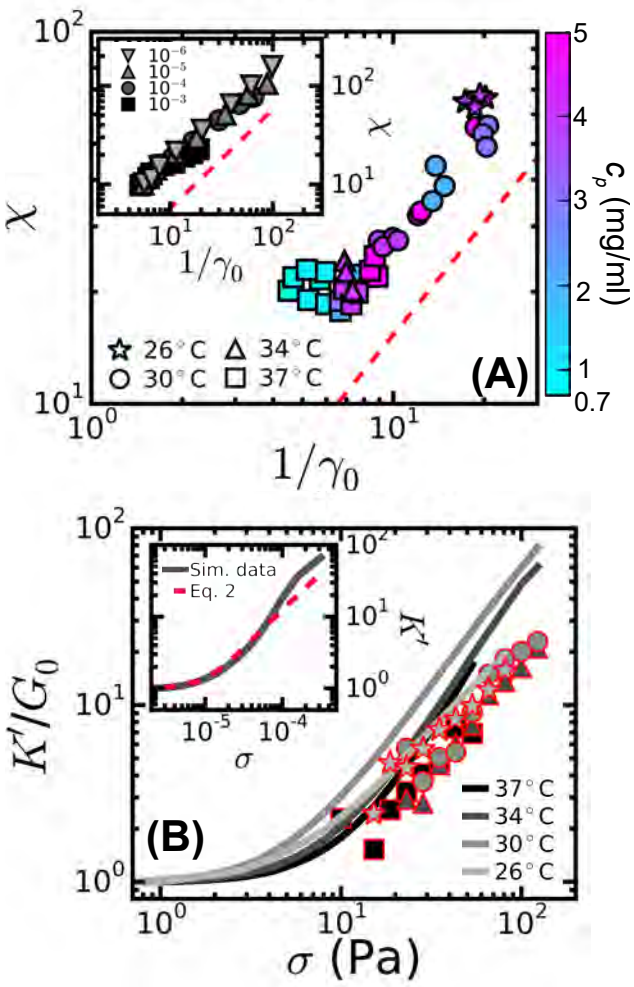

Figure 9: The self-generated normal stress stabilizes collagen networks and controls the initial strain-stiffening response. (A) Both in experiments (main plot) and in simulations (inset), the susceptibility χ determined from stress-stiffening curves (symbols) is linear in $1/\gamma_0$ (dashed lines). Collagen gels were polymerized at temperatures between 26 and 37°C and collagen concentrations between 0.7 and 5 mg/ml (blue-pink) (see legend and color bar on the right). Simulations in the inset were performed for different $\widetilde{\kappa}$ values (see legend) and for $\langle z \rangle$ between 3 and 3.87 (see Table S2 in SI). (B) The stress-stiffening response of 4 mg/ml collagen networks polymerized at temperatures ranging from 26 to 37°C is correctly predicted by Eq. 2 (red symbols, calculated using measurements of the normal stress as input) to within a factor of 2. (B, inset) The simulations likewise show agreement between simulated K' values (gray line) and calculations from the normal stress using Eq. 2 (red dashed line), as exemplified for a network with $\widetilde{\kappa} = 10^{-4}$ and $\langle z \rangle = 3.2$. In panel (A), all individual measurements (at least 3 per conditions) are plotted, while in panel B representative curves are shown.

Recent simulations suggest that there is a fundamental connection between the elastic modulus K' and the self-generated normal stress, σ_N in sub-marginal fibrous networks under shear (20, 40). Specifically, it was shown that K' grows in direct proportion to σ_N:

$$K' \simeq G_0 + \chi|\sigma_N| \tag{2}$$

where χ is the susceptibility. It was hypothesized that the normal stress stabilizes the network once the network is strained out of the linear regime ($\gamma > \gamma_0$) and before it undergoes a strain-driven transition to a stretch-dominated regime (at γ_c). Here we experimentally test this intriguing hypothesis by measuring the normal stress that collagen gels exert on the top plate of the rheometer as a function of the applied shear stress. As shown in Fig. 8A, shearing indeed induces a significant negative

normal stress that increases in magnitude with increasing shear stress. We observe this effect for all collagen gels polymerized at concentrations above $\sim$1 mg/ml and polymerization temperatures of 26°C or higher. We were unable to obtain measurable normal stress signals for collagen gels polymerized at 22°C, likely because we are unable to reach large enough strains to enter far enough into the nonlinear regime. We note that we always observed a nonzero normal stress even at small strain, which is likely dominated by the surface tension of the sample at its edge (38). Since this effect is not related to the elastic properties of the collagen network itself, we subtracted this offset from the normal stress data.

To test the validity of the model, we first verified that K' exhibits the expected linear dependence on σ_N by plotting data for different collagen concentrations and polymerization temperatures together. As shown in Fig. 8B, we indeed find a linear dependence of K' on σ_N. According to Eq. 2, we should in principle be able to determine the susceptibility χ from a linear fit to these data. However, since σ_N was rather noisy, especially at collagen concentrations below 2 mg/ml, we used an alternative approach. According to the simulations, right at the point where strain-stiffening sets in, the shear stress and the normal stress are comparable in magnitude (37, 40, 55). We can therefore rewrite Eq. 2 as $K'/\sigma_0 \simeq \chi$. Using the σ_0-values we already determined from stress-stiffening curves, we find that χ is linear in $1/\gamma_0$ (see Fig. 9A)), in line with the simulations (inset). Finally, taking these values for χ as input, we tested whether the stress-stiffening behavior of collagen networks is controlled by normal stress as predicted by Eq. 2. As shown in Fig. 9B, we indeed observe a reasonable correspondence between the stiffening behavior predicted on the basis of the measured normal stress response (lines) and the measured stiffening response (symbols) for 4 mg/ml collagen networks polymerized at temperatures of 26°C and above. We observe a similarly good agreement at other collagen concentrations (Fig S9 in SI). We consistently observe a factor 2 difference between theory and experiment, perhaps because Eq. 2 is only valid at stresses below σ_c. Altogether, the experiments provide strong support for the hypothesis made on the basis of simulations that a shear-induced normal force governs the nonlinear elasticity of collagen gels at intermediate strains between γ_0 and γ_c. Moreover, this agreement provides further evidence that elastic fiber network models provide an appropriate description of collagen elasticity over a wide range of assembly conditions.

4 Discussion

We combined experiments and computational modelling to elucidate the origin of the nonlinear elastic properties of fibrillar collagen networks. By varying the polymerization temperature between 22 and 37°C and the collagen monomer concentration between 0.5 and 5 mg/ml, we obtained collagen networks with an architecture ranging from a sparse meshwork of thick collagen fibril bundles to a dense meshwork of thin collagen fibrils. We modelled the networks as random networks of stiff fibers with an average local connectivity between 3 (branch points) and 4 (junctions of crosslinked fibers). We showed that the model provides a self-consistent description of all aspects of the nonlinear elastic response of collagen networks (i.e. G_0, γ_0, γ_c, β, and the relation between shear modulus and normal stress) with reasonable parameter values for the average connectivity $\langle z \rangle$ and the fiber Young's modulus E. We furthermore showed that the quantitative agreement between theory and experiment holds over the entire concentration range and all polymerization temperatures between 26 and 37°C. Only for networks formed at 22°C we could not use the model since these networks were too heterogeneous and exhibited marked inelastic behavior. Several recent studies likewise identified inelastic behavior in collagen networks (57, 58), which allows cells to align and bundle collagen fibers by applying traction forces (59–61). Our data suggest that the extent to which collagen behaves inelastically can be tuned by the polymerization temperature, probably through a modulation of the hydrophobic interactions that dominate collagen association. It will be an interesting challenge to include such inelastic effects in our random network model by extending it with transient fiber-fiber bonding.

Our work suggests that microscopic properties of collagen can be inferred from macroscopic rheology data by comparing experiments against theoretical predictions for fibrous networks. The conditions under which this approach is valid are well-defined and easily verified by microscopy and rheology experiments: the network needs to be isotropic, athermal, elastic, and subisostatic (i.e., $\langle z \rangle$ needs to be below 6).

We propose that the bending rigidity of the fibrils can be inferred from the linear elastic modulus, G_0. We were able to explain the dependence of G_0 on collagen concentration and polymerization temperature with a single value for the fibril Young's modulus of 1.1 MPa. It is difficult to directly validate this number, because this requires challenging *in situ* micromanipulation measurements on individual collagen fibrils within 3D networks. Until now, micromanipulation measurements have been restricted to isolated collagen fibrils. Furthermore, those measurements vary over a wide range, depending on whether the fibers are reconstituted from purified collagen or extracted from tissue, on sample preparation, and on the measurement technique. A direct comparison to literature values is therefore difficult. Values for (hydrated) native collagen fibrils range from 2-5 MPa (51), to 10-30 MPa (53), 50-120 MPa (48, 49, 52) and even 100-360 MPa (47). The few reports we are aware of where reconstituted collagen fibrils were used report smaller moduli, of just a few kPa (62) or several MPa (53). It is not surprising that reconstituted fibrils would be softer than native fibrils, given that they are much less crosslinked (63, 64). In

light of the existing literature, we consider the value of 1.1 MPa we infer for the Young's modulus of reconstituted collagen I fibers as reasonable. In future it will be interesting to perform micromanipulation measurements on fibrils within 3D networks using optical or magnetic tweezers, to test the Young's modulus under physiologically relevant assembly conditions.

Our findings suggest that also the nonlinear elastic response of collagen networks can reveal microscopic properties of the networks, specifically the average coordination number $\langle z \rangle$. The strain-stiffening response has two phases, with an onset of stiffening at a strain γ_0, and a strain-controlled transition from a bend-dominated regime to a stretch-dominated elastic regime at a strain γ_c. We observed that γ_0 and γ_c both increase with increasing polymerization temperature. In the context of the model, this observation tells us that $\langle z \rangle$ decreases from 3.5 to 3 on going from 26 to 37°C. We reach the same conclusion when we consider the linear modulus G_0, which drops on going from 26 to 30°C, and the stress-stiffening exponent, β, which increases with increasing polymerization temperature. The structure of collagen networks is known to be kinetically determined. With increasing temperature, we expect an increased rate of nucleation and growth of collagen fibers, which will increase the likelihood of branching. Networks formed at 37°C have $\langle z \rangle$ close to 3, consistent with a highly branched network, over a range of concentrations between 2 and 5 mg/ml. Indeed, with increasing temperatures, we expect an increased rate of nucleation and growth of collagen fibers, which will increase the likelihood of branching. Below 2 mg/ml, we find $\langle z \rangle$ values below 3, suggesting the presence of dangling (elastically inactive) ends. Admittedly, the determination of $\langle z \rangle$ is currently model-dependent. We find that it is difficult to determine $\langle z \rangle$ precisely from imaging alone. Imaging cannot distinguish whether fibers form a true junction or are merely entangled or in close proximity. Moreover, it is difficult to determine whether the fiber ends are crosslinked to other fibers or dangling. A further issue is the difficulty in reliably tracing all fibers in dense 3D networks (26, 65, 66). In the future, it may be possible to solve these issues by using time-lapse imaging or micromanipulation experiments to test whether an apparent junction of two fibers is a crosslinked pair or just an entangled pair. Our work suggests that rheological measurements meanwhile provide a robust and convenient assay to measure the ensemble-averaged network connectivity. At the same time, the sensitivity of the rheology to small changes in connectivity can explain the diversity of concentration dependencies observed in studies performed with different collagen batches and assembly conditions, with power law dependencies of G_0 on concentration with exponents varying between 1 and 3 (18, 19, 32–36).

Our model provides a mechanistic basis for explaining the strain-stiffening behavior that is characteristic of collagen networks and collagenous tissues. Earlier computational studies had suggested that strain-stiffening originates from a transition from bending-dominated elasticity at low strain to a stretch-dominated elasticity regime at high strain (67). However, here we showed that collagen networks already stiffen substantially, well before the transition to the stretch-dominated state occurs. Thus, the initial strain-stiffening response that sets in at γ_0 is actually not caused by a bend-to-stretch transition. A recent theoretical study put forward the hypothesis based on simulation data that the initial stiffening is induced by a self-generated normal stress (20, 40). Here, we experimentally confirm this hypothesis. We find that sheared collagen networks indeed develop a large negative (contractile) normal stress and that the elastic modulus K' grows in direct proportion to the magnitude of this normal stress. It is only for strains above γ_c that the networks undergo a transition to a rigid stretch-dominated elastic regime (25, 29).

The microscopic model we propose opens up several interesting avenues of future research. First, our findings provide a starting point to develop multi-scale models of collagen networks that incorporate the different hierarchical levels of structure. In this paper, we coarse-grained the collagen fibers as uniform elastic beams. This approach allows us to model the effective elastic properties of the fibers, but it cannot account for the mechanical anisotropy of collagen fibers associated with their bundle-like structure (68, 69) nor for strain-dependent changes in their molecular packing (9, 70). Depending on the required level of detail, the fibers could be modelled as Timoshenko beams to account for intrafibrillar shear (69), or one could even integrate the model with constitutive relations determined from full-atom simulations to account for the viscoelastic properties of the fibers (22) and strain-induced fiber lengthening via subunit sliding (20).

Second, our findings provide a quantitative framework to understand how auxiliary extracellular matrix proteins regulate the structure and mechanics of collagen networks. While collagen I is the most abundant type of collagen in noncartilaginous tissues ($> 90\%$), it nevertheless always forms 'heterotypic' fibrils together with other fibrillar collagens such as collagens III and V and noncollagenous molecules such as glycosaminoglycans. This co-assembly is thought to provide an essential mechanism for regulating the diameter of the fibrils and tailoring collagen networks for the specific biomechanical requirements of different adult tissues and of remodelling tissues (1). Using the random network model it should now be possible to relate the mechanical properties of collagen networks to the underlying changes in structure at both the fibril and network scale.

Third, our findings provide a quantitative framework to investigate the mechanobiology of cell-matrix interactions. Cell-seeded collagen networks are widely used as extracellular matrix model systems for tissue morphogenesis, wound healing, cell migration, and cancer biology (10, 11). The elastic modulus of collagen networks was shown to influence many cell functions such as cell migration and proliferation (17, 71, 72). Our work facilitates systematic studies of this mechanoregulation by making it possible to design the network structure to achieve a desired elastic response. Our work also facilitates measurements of the transmission of forces generated by cells cultured in collagen networks. Recently several methods have

been proposed to infer the traction forces that cells exert on the collagen matrix at focal adhesion sites from imaging-based measurements of the matrix strain (61, 73, 74). This has been a challenging problem due to the fibrous architecture of collagen networks, which causes cells to stiffen the matrix around them (75, 76) and makes force transmission long-ranged (61, 77). Our findings strongly support the validity of using athermal random network models to provide a quantitative relation between stresses and strains in collagen matrices.

5 Conclusion

Our findings show that models of disordered networks of elastic fibers provide a unifying framework to understand the relation between collagen network mechanics and microstructure over a wide range of assembly conditions as long as the network structure is isotropic and sufficiently uniform. Interestingly, our work suggests that macroscopic measurements of the nonlinear elastic behavior are able to reveal microscopic information about the average network connectivity, a parameter that is difficult to determine reliably from microscopy images. It will be important in future work to find model-independent methods of measuring the network connectivity to validate this conclusion based on imaging. Our work establishes a strong basis to predict the elastic properties of more physiologically relevant collagen systems, where the fibril diameter is regulated by co-polymerization of collagen I with other fibril-forming collagens and glycosaminoglycans. Moreover, our study provides a quantitative framework to design collagen networks with desired mechanical properties, which is useful for biophysical studies on the mechanoregulation of cell migration, wound healing, and tissue morphogenesis. Our model is generally applicable to fibrous networks provided that the networks are isotropic, athermal, and subisostatic. There are many biological materials that fulfil these criteria in addition to collagen, including fibrin that mediates blood clotting in animals and cellulose that provides support to plant and tree tissues.

6 SUPPLEMENTARY INFORMATION

An online supplement to this article with a description of the Materials and Methods, 11 figures, and 2 tables with supplementary data can be found by visiting BJ Online at http://www.biophysj.org.

7 Supporting Citations

References (78–87) appear in the Supplementary Material.

8 Authors Contributions

KAJ, AJL, AS, GHK and FCM designed research; KJ, AJL, AS and RR performed research and analyzed data; all authors wrote the paper.

9 ACKNOWLEDGMENTS

The authors thank B. Vos for analyzing and discussing the turbidity data and F. Burla for critically reading the manuscript. F.C.M. was supported in part by the National Science Foundation (Grant PHY-1427654). This work was further supported by the Foundation for Fundamental Research on Matter (FOM), which is part of the Netherlands Organisation for Scientific Research (NWO), and by NanoNextNL, a micro and nanotechnology programme of the Dutch Government and 130 partners.

References

1. Fratzl, P., editor, 2008. Collagen Structure and Mechanics. Springer Science+Business Media.
2. Kjaer, M., H. Langberg, K. Heinemeier, M. Bayer, M. Hansen, L. Holm, S. Doessing, M. Kongsgaard, M. Krogsgaard, and S. Magnusson, 2009. From mechanical loading to collagen synthesis, structural changes and function in human tendon. Scand. J. Med. Sci. Sports 19:500–510.
3. Boote, C., C. Kamma-Lorger, S. Hayes, J. Harris, M. Burghammer, J. Hiller, N. Terril, and K. Meek, 2011. Quantification of collagen organization in the peripheral human cornea at micron-scale resolution. Biophys. J. 101:33–42.
4. Mouw, J., G. Ou, and V. Weaver, 2014. Extracellular matrix assembly: a multiscale deconstruction. Nat. Rev. Mol. Cell Biol. 15:771–785.
5. Kai, F., H. Laklai, and V. Weaver, 2016. Force Matters: Biomechanical Regulation of Cell Invasion and Migration in Disease. Trends

Cell Biol. 26:486–497.
6. Fung, Y., 1984. Structure and Stress-Strain Relationship of Soft Tissues. Amer. Zool. 24:13–22.
7. Shadwick, R. E., 1999. Mechanical design in arteries. The Journal of Experimental Biology 202:3305–3313.
8. Orgel, J. P., T. C. Irving, A. Miller, and T. J.Wess, 2006. Microfibrillar structure of type I collagen *in situ*. PNAS 103:9001–9005.
9. Misof, K., G. Rapp, and P. Fratzl, 1997. A new molecular model for collagen elasticity based on synchrotron X-ray scattering evidence. Biophys. J. 72:1376–1381.
10. Grinnel, F., and W. M. Petroll, 2010. Cell Motility and Mechanics in Three-Dimensional Collagen Matrices. Annual Review of Cell and Developmental Biology 26:335–361.
11. Brown, R. A., 2013. In the beginning there were soft collagen-cell gels: towards better 3D connective tissue models? Experimental Cell Research 319:2460–2469.
12. Roeder, B. A., K. Kokini, J. E. Sturgis, J. P. Robinson, and S. L. Voytik-Harbin, 2002. Tensile Mechanical Properties of Three-Dimensional Type I Collagen Extracellular Matrices With Varied Microstructure. Transactions of the ASME 124:214–222.
13. Raub, C. B., J. Unruh, V. Suresh, T. Krasieva, T. Lindmo, E. Gratton, B. J. Tromberg, and S. C. George, 2008. Image Correlation Spectroscopy of Multiphoton Images Correlates with Collagen Mechanical Properties. Biophys. J. 94:2361–2373.
14. Sapudom, J., S. Rubner, S. Martin, T. Kurth, S. Riedel, C. T. Mierke, and T. Pompe, 2015. The phenotype of cancer cell invasion controlled by fibril diameter and pore size of 3D collagen networks. Biomacromolecules 52:367–375.
15. Raub, C. B., V. Suresh, T. Krasieva, J. Lyubovitsky, J. D. Mih, A. J. Putnam, B. J. Tromberg, and S. C. George, 2007. Noninvasive Assessment of Collagen Gel Microstructure and Mechanics Using Multiphoton Microscopy. Biophys. J. 92:2212–2222.
16. Hwang, Y.-J., and J. G. Lyubovitsky, 2011. Collagen hydrogel characterization: multi-scale and multi-modality approach. Analytical Methods 3:529–536.
17. Wolf, K., M. te Lindert, M. Krause, S. Alexander, J. te Riet, A. L. Willis, R. M. Hoffman, C. G. Figdor, S. J. Weiss, and P. Friedl, 2013. Physical limits of cell migration: Control by ECM space and nuclear deformation and tuning by proteolysis and traction force. Journal of Cell Biology 201:1069–1084.
18. Motte, S., and L. J. Kaufman, 2012. Strain Stiffening in Collagen I Networks. Biopolymers 99:35–46.
19. Vader, D., A. Kabla, D. Weitz, and L. Mahadevan, 2009. Strain-Induced Alignment in Collagen Gels. PLoS ONE 4:e5902.
20. Licup, A. J., S. Münster, A. Sharma, M. Sheinman, L. M. Jawerth, B. Fabry, D. A. Weitz, and F. C. MacKintosh, 2015. Stress controls the mechanics of collagen networks. PNAS 112:9573–9578.
21. Kurniawan, N. A., L. H. Wong, and R. Rajagopalan, 2012. Early Stiffening and Softening of Collagen: Interplay of Deformation Mechanisms in Biopolymer Networks. Biomacromolecules 13:691–698.
22. Gautieri, A., S. Vesentini, A. Redaelli, and M. J. Buehler, 2011. Hierarchical structure and nanomechanics of collagen microfibrils from the atomistic scale up. Nano Lett. 11:757–766.
23. Varma, S., J. P. Orgel, and J. D. Schieber, 2016. Nanomechanics of Type I Collagen. Biophys. J. 111:50–56.
24. Chandran, P. L., and V. H. Barocas, 2006. Affine versus non-affine fibril kinematics in collagen networks: theoretical studies of network behavior. J. Biomech. Eng. 128:259–270.
25. Sharma, A., A. Licup, K. Jansen, R. Rens, M. Sheinman, G. Koenderink, and F. MacKintosh, 2016. Strain-controlled criticality governs the nonlinear mechanics of fibre networks. Nature Physics 12:584–587.
26. Lindström, S. B., D. A. Vader, A. Kulachenko, and D. A. Weitz, 2010. Biopolymer network geometries: Characterization, regeneration, and elastic properties. PRE 82:051905.
27. Maxwell, J., 1864. On the calculation of the equilibrium and stiffness of frames. Philosophical Magazine 27:294–299.
28. Broedersz, C. P., X. Mao, T. C. Lubensky, and F. C. MacKintosh, 2011. Criticality and isostaticity in fibre networks. Nature Physics 7:983–988.
29. Sharma, A., A. Licup, R. Rens, M. Vahabi, K. Jansen, G. Koenderink, and F. MacKintosh, 2016. Strain-driven criticality underlies nonlinear mechanics of fibrous networks. PRE 94:042407.
30. Kroy, K., and E. Frey, 1996. Force-Extension Relation and Plateau Modulus for Wormlike Chains. PRL 77:306.
31. Satcher, R., and C. Dewey, 1996. Theoretical estimates of mechanical properties of the endothelial cell cytoskeleton. Biophys. J. 71:109–118.
32. li Yang, Y., L. M. Leone, and L. J. Kaufman, 2009. Elastic Moduli of Collagen Gels Can Be Predicted from Two-Dimensional Confocal Microscopy. Biophys. J. 97:2051–2060.
33. Kreger, S., B. Bell, J. Bailey, E. Stites, J. Kuske, B. Waisner, and S. Voytik-Harbin, 2010. Polymerization and Matrix Physical Properties as Important Design Considerations for Soluble Collagen Formulations. Biopolymers 93:690–707.
34. Piechocka, I. K., A. S. van Oosten, R. G. Breuls, and G. H. Koenderink, 2011. Rheology of Heterotypic Collagen Networks. Biomacromolecules 12:2797–2805.
35. Velegol, D., and F. Lanni, 2001. Cell Traction Forces on Soft Biomaterials. I. Microrheology of Type I Collagen gels. Biophys. J. 81:1786–1792.
36. Miron-Mendoza, M., J. Seemann, and F. Grinnell, 2010. The differential regulation of cell motile activity through matrix stiffness and porosity in three dimensional collagen matrices. Biomaterials 31:6425–6435.
37. Janmey, P. A., M. E. McCormick, S. Rammensee, J. L. Leight, P. C. Georges, and F. C. MacKintosh, 2006. Negative normal stress in semiflexible biopolymer gels. Nature Materials 6:48–51.
38. de Cagny, H., B. Vos, M. Vahabi, N. Kurniawan, M. Doi, G. Koenderink, F. MacKintosh, and D. Bonn, 2016. Porosity governs normal

stresses in polymer gels. PRL 117:217802.
39. Poynting, J. H., 1909. On Pressure Perpendicular to the Shear Planes in Finite Pure Shears, and on the Lengthening of Loaded Wires When Twisted. Proceedings of the Royal Society A: Mathematical, Physical and Engineering Sciences 82:546–559.
40. Licup, A. J., A. Sharma, and F. C. MacKintosh, 2016. Elastic regimes of subisostatic athermal fiber networks. PRE 93:012407.
41. Forgacs, G., S. A. Newman, B. Hinner, C. W. Maier, and E. Sachmann, 2003. Assembly of collagen Matrices as a phase transition revealed by structural and rheologic studies. Biophys. J. 84:1272–1280.
42. Jones, C. A. R., L. Liang, D. Lin, Y. Jiao, and B. Sun, 2014. The spatial-temporal characteristics of type I collagen-based extracellular matrix. Soft Matter 10:8855–8863.
43. Zhu, J., and L. J. Kaufman, 2014. Collagen I Self-Assembly: Revealing the Developing Structures that Generate Turbidity. Biophys. J. 106:1822–1831.
44. Ferri, F., G. R. Calegari, M. Molteni, B. Cardinali, D. Magatti, and M. Rocco, 2015. Size and density of fibers in fibrin and other filamentous networks from turbidimetry: beyond a revisited Carr-Hermans method, accounting for fractality and porosity. Macromolecules 48:5423–5432.
45. Broedersz, C., M. Sheinman, and F. MacKintosh, 2012. Filament-Length-Controlled Elasticity in 3D Fiber Networks. PRL 108:078102.
46. Bartsch, T. F., M. D. Kochanczyk, E. N. Lissek, J. R. Lange, and E. L. Florin, 2016. Nanoscopic imaging of thick heterogeneous soft-matter structures in aqueous solution. Nat. Commun. 7:12729.
47. Dutov, P., O. Antipova, S. Varma, J. P. Orgel, and J. D. Schieber, 2016. Measurement of Elastic Modulus of Collagen Type I Single Fiber. PLoS One 11:e0145711.
48. Shen, Z. L., H. Kahn, R. Ballarini, and S. J. Eppell, 2011. Elastic properties of isolated collagen fibrils. Biophys. J. 100:2008–2015.
49. Yang, L., K. van der Werf, P. Dijkstra, J. Feijen, and M. Bennink, 2012. Micromechanical analysis of native and cross-linked collagen type I fibrils supports the existence of microfibrils. Journal of the Mechanical Behavior of Biomedical Materials 6:148–158.
50. Liu, Y., R. Ballarini, and S. J. Eppell, 2016. Tension tests on mammalian collagen fibrils. Interface Focus 6:20150080.
51. Grant, C. A., D. J. Brockwell, S. E. Radford, and N. H. Thomson, 2009. Tuning the elastic modulus of hydrated collagen fibrils. Biophys. J. 97:2985–2992.
52. Aifantis, K. E., S. Shrivastava, and G. M. Odegard, 2011. Transverse mechanical properties of collagen fibers from nanoindentation. J Mater Sci Mater 22:1375–1381.
53. Baldwin, S. J., A. S. Quigley, C. Clegg, and L. Kreplak, 2014. Nanomechanical mapping of hydrated rat tail tendon collagen I fibrils. Biophys. J. 107:1794–1801.
54. Rens, R., M. Vahabi, A. Licup, F. MacKintosh, and A. Sharma, 2016. Nonlinear Mechanics of Athermal Branched Biopolymer Networks. J. Phys Chem B 120:5831–41.
55. Conti, E., and F. C. MacKintosh, 2009. Cross-Linked Networks of Stiff Filaments Exhibit Negative Normal Stress. PRL 102:088102.
56. Cioroianu, A., and C. Storm, 2013. Normal stresses in elastic networks. Phys Rev E Stat Nonlin Soft Matter Phys 88:052601.
57. Münster, S., L. M. Jawerth, B. A. Leslie, J. I. Weitz, B. Fabry, and D. A. Weitz, 2013. Strain history dependence of the nonlinear stress response of fibrin and collagen networks. PNAS 110:12197–12202.
58. Nam, S., K. H. Hu, M. J. Butte, and O. Chaudhuri, 2016. Strain-enhanced stress relaxation impacts nonlinear elasticity in collagen gels. PNAS 113:5492–5499.
59. Mohammadi, H., P. D. Arora, C. A. Simmons, P. A. Janmey, and C. A. McCullock, 2014. Inelastic behaviour of collagen networks in cell-matrix interactions and mechanosensation. J. R. Roc. Interface 12:20141074.
60. Nam, S., J. Lee, D. Brownfield, and O. Chaudhuri, 2016. Viscoplasticity Enables Mechanical Remodeling of Matrix by Cells. Biophys. J. 111:2296–2308.
61. Hall, M., F. Alisafaei, E. Ban, X. Feng, C. Hui, V. Shenoy, and M. Wu, 2016. Fibrous nonlinear elasticity enables positive mechanical feedback between cells and ECMs. PNAS 113:14043–14048.
62. Doyle, A. D., N. Carvajal, A. Jin, K. Matsumoto, and K. M. Yamada, 2015. Local 3D matrix microenvironment regulates cell migration through spatiotemporal dynamics of contractility-dependent adhesions. Nature Communications 6:8720.
63. Eyre, D., and J. Wu, 2005. Collagen cross-links. Top Curr Chem 247:207–229.
64. Gautieri, A., F. Passini, U. Silván, M. Guizar-Sicairos, G. Carimati, P. Volpi, M. Moretti, H. Schoenhuber, A. Redaelli, M. Berli, and J. Snedeker, 2016. Advanced glycation end-products: Mechanics of aged collagen from molecule to tissue. Matrix Biol. 59:95–108.
65. Reese, S., N. Farhang, R. Poulson, G. Parkman, and J. Weiss, 2016. Nanoscale Imaging of Collagen Gels with Focused Ion Beam Milling and Scanning Electron Microscopy. Biophys. J. 111:1797–1804.
66. Xu, T., D. Vavylonis, F.-C. Tsai, G. Koenderink, W. Nie, E. Yusul, I.-J. Lee, J.-Q. Wu, and X. Huang, 2015. SOAX: A software for quantification of 3D biopolymer networks. Scientific Reports 5:9081.
67. Onck, P., T. Koeman, T. van Dillen, and E. van der Giessen, 2005. Alternative Explanation of Stiffening in Cross-linked Semiflexible networks. PRL 95:178102.
68. Heim, A., T. Koob, and W. Matthews, 2007. Low strain nanomechanics of collagen fibrils. Biomacromolecules 8:3298–3301.
69. Yang, L., K. van der Werf, C. Fitié, M. Bennink, P. Dijkstra, and J. Feijen, 2008. Mechanical properties of native and cross-linked type I collagen fibrils. Biophys. J. 94:2204–2211.
70. Masic, A., L. Bertinetti, R. Schuetz, S. Chang, T. Metzger, M. Buehler, and P. Fratzl, 2015. Osmotic pressure induced tensile forces in tendon collagen. Biophys. J. 6:5942.

71. Bott, K., Z. Upton, K. Schrobback, M. Ehrbar, J. Hubbell, M. Lutolf, and S. Rizzi, 2013. The effect of matrix characteristics on fibroblast proliferation in 3D gels. Biomaterials 31:8454–64.
72. Lang, N. R., K. Skodzek, S. Hurst, A. Mainka, J. Steinwachs, J. Schneider, K. E. Aifantis, and B. Fabry, 2015. Biphasic response of cell invasion to matrix stiffness in three-dimensional biopolymer networks. Acta Materialia 13:61–67.
73. Steinwachs, J., C. Metzner, K. Skodzek, N. Lang, I. Thievessen, C. Mark, S. Münster, K. Aifantis, and B. Fabry, 2016. Three-dimensional force microscopy of cells in biopolymer networks. Nat Methods. 13:171–6.
74. Liang, L., C. Jones, S. Chen, B. Sun, and Y. Jiao, 2016. Heterogeneous force network in 3D cellularized collagen networks. Physical Biology 13:066001.
75. Jones, C. A., M. Cibula, J. Feng, E. A. Kmacik, D. H. McIntyre, H. Levine, and B. Sun, 2015. Micromechanics of cellularized biopolymer networks. PNAS E5117–E5112.
76. van Helvert, S., and P. Friedl, 2016. Strain Stiffening of Fibrillar Collagen during Individual and Collective Cell Migration Identified by AFM Nanoindentation. ACS Appl Mater Interfaces 8:21946–55.
77. Xu, X., and S. Safran, 2015. Nonlinearities of biopolymer gels increase the range of force transmission. Phys Rev E Stat Nonlin Soft Matter Phys. 92:032728.
78. Newman, S., M. C. C. Allain, G. Forgacs, and D. Beysens, 1997. Viscosity and Elasticity During Collagen Assembly In Vitro: Relevance to Matrix-Driven Translocation. Biopolymers 41:337–347.
79. Wood, G., and M. Keech, 1960. The Formation of Fibrils from Collagen Solutions. 1. The Effect of Experimental Conditions: Kinetic and Electron-Microscope Studies. Biochemical Journal 75:588–589.
80. Brokaw, J., C. Doillon, R. Hahn, D. Birk, R. Berg, and F. Silver, 1985. Turbidimetry and morphological studies of type I collagen fiber assembly in vitro and the influence of fibronectin. Int. J. Biol. Macromol. 7:135–140.
81. Wess, T., 2005. Collagen fibril form and function. Adv. Protein Chem. 341–374.
82. Baradet, T. C., J. C. Haselgrove, and J. W. Weisel, 1995. Three-Dimensional Reconstruction of Fibrin Clot Networks from Stereoscopic Intermediate Voltage Electron Microscope Images and Analysis of Branching. Biophys. J. 68:1551–1560.
83. Gersh, K. C., C. Nagaswami, and J. W. Weisel, 2009. Fibrin network structure and clot mechanical properties are altered by incorporation of erythrocytes. Thromb. Haemost. 102:1169–1175.
84. de Wild, M., W. Pomp, and G. H. Koenderink, 2013. Thermal Memory in Self-Assembled Collagen Fibril Networks. Biophys. J. 105:200–210.
85. Landau, L., and E. Lifshiftz, editors, 1970. Theory of elasticity. Pergamon Press, Oxford, 2nd edition.
86. Carr, M. E., and J. Hermans, 1978. Size and Density of Fibrin Fibers from Turbidity. Macromolecules 11:46–50.
87. Yeromonahos, C., B. Polack, and F. Caton, 2010. Nanostructure of the Fibrin Clot. Biophys. J. 99:2018–2027.

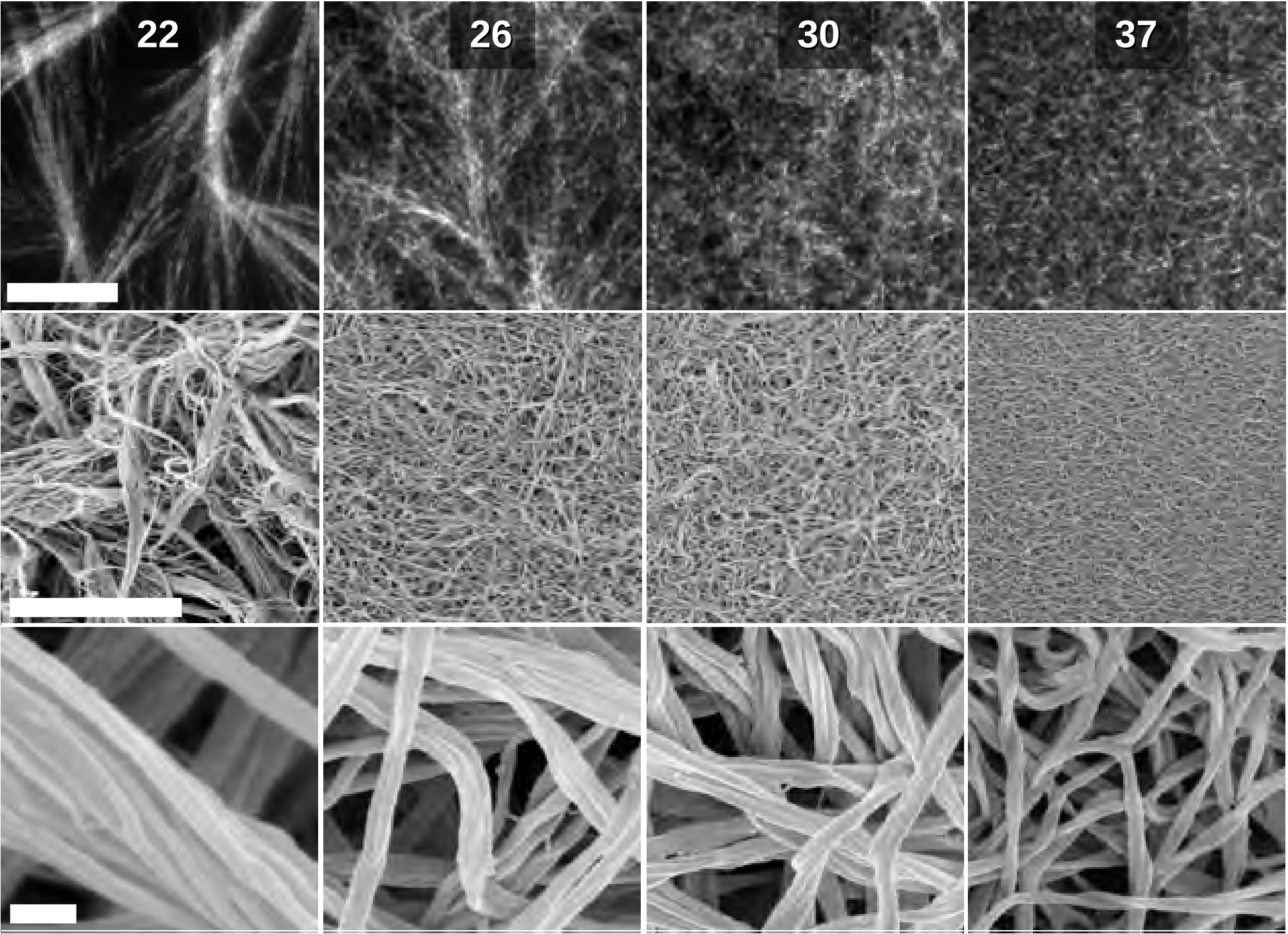
22
26
30
37

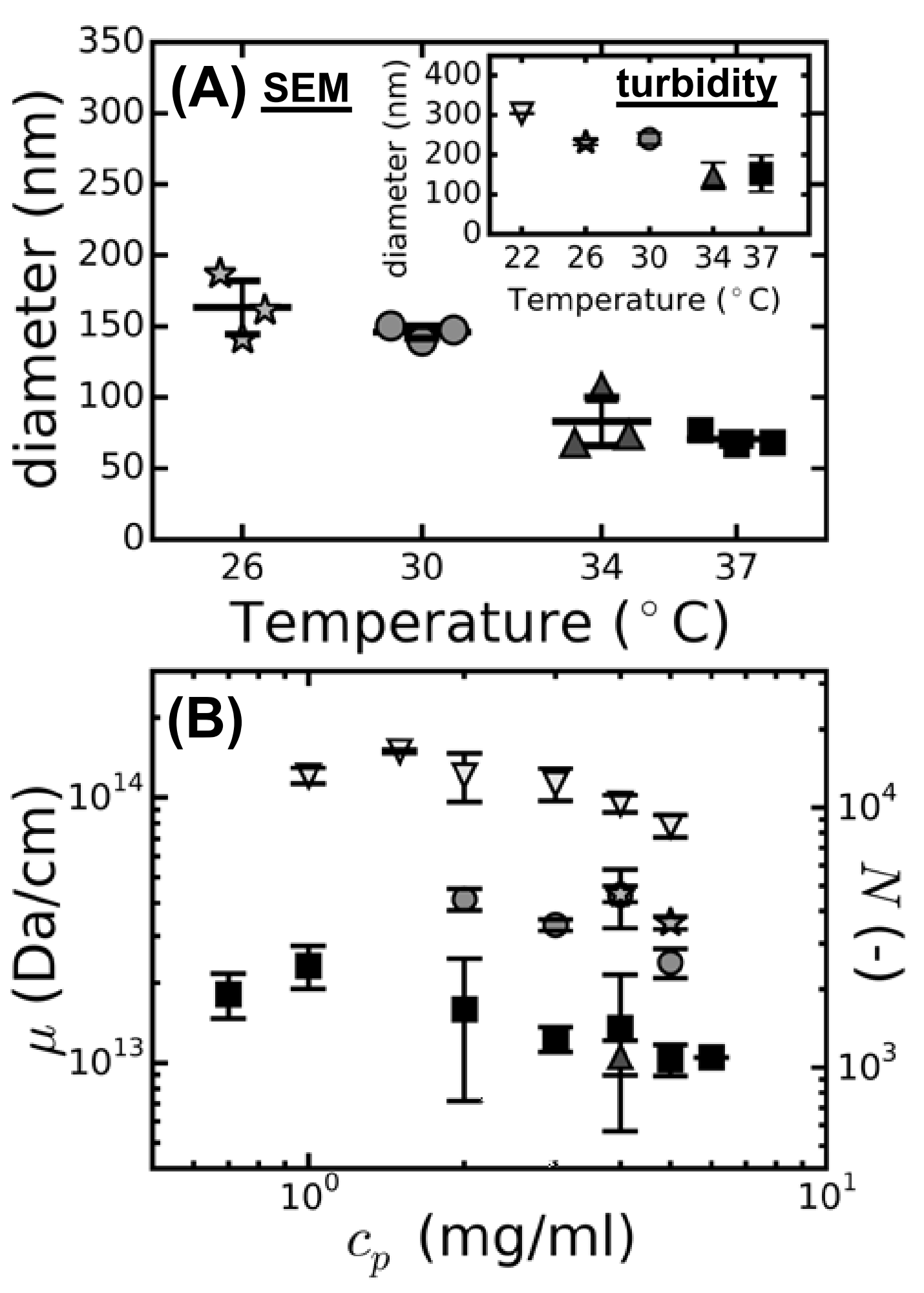
(A) SEM
diameter (nm)
350
300
250
200
150
100
50
0
26
30
34
37
Temperature (°C)
turbidity
diameter (nm)
400
300
200
100
0
22
26
30
34
37
Temperature (°C)
(B)
μ (Da/cm)
10^{14}
10^{13}
N (-)
10^{4}
10^{3}
10^{0}
10^{1}
c_p (mg/ml)

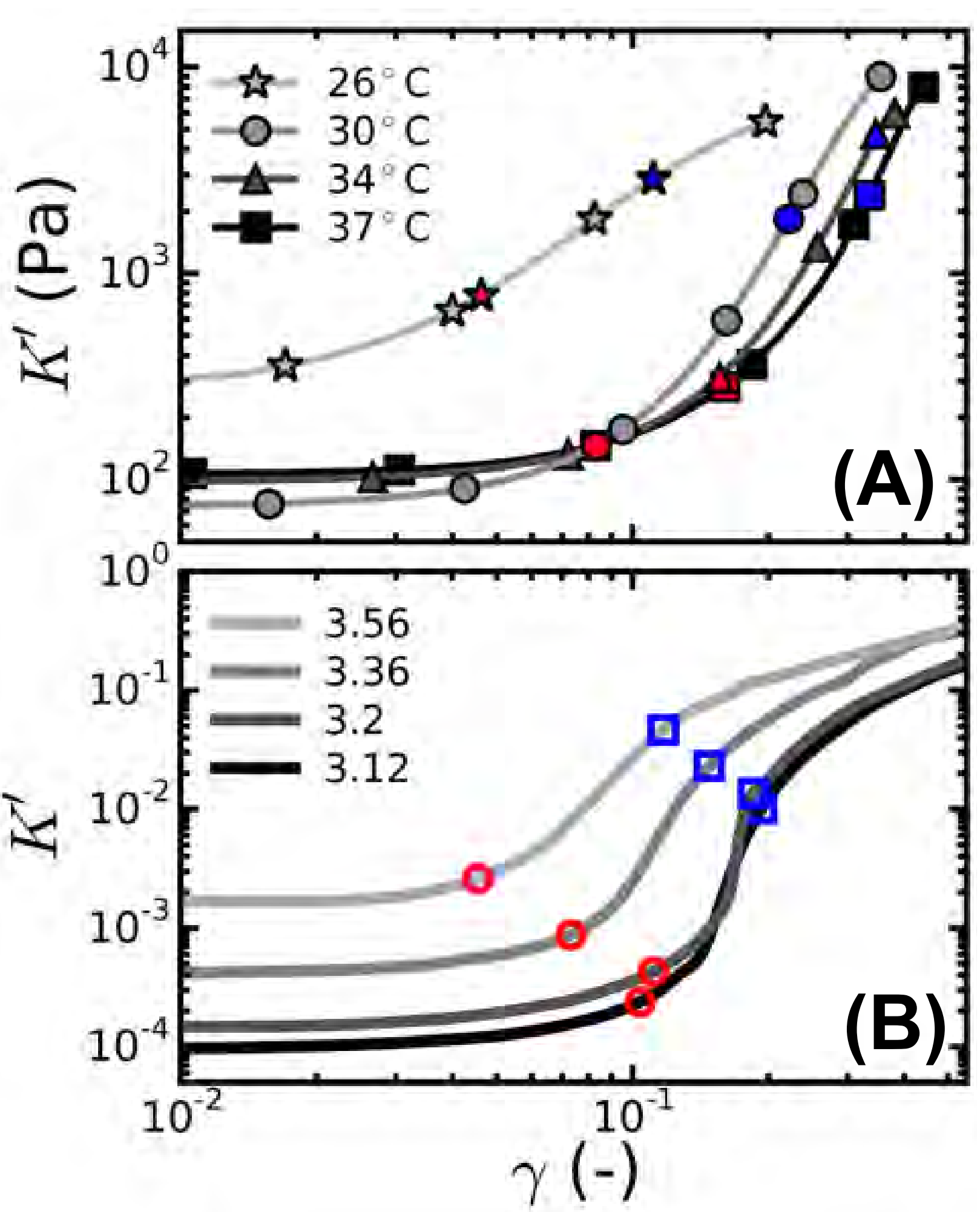
10^4
10^3
10^2
10^0
K' (Pa)
26°C
30°C
34°C
37°C
(A)
10^0
10^{-1}
10^{-2}
10^{-3}
10^{-4}
K'
3.56
3.36
3.2
3.12
(B)
10^{-2}
10^{-1}
γ (-)

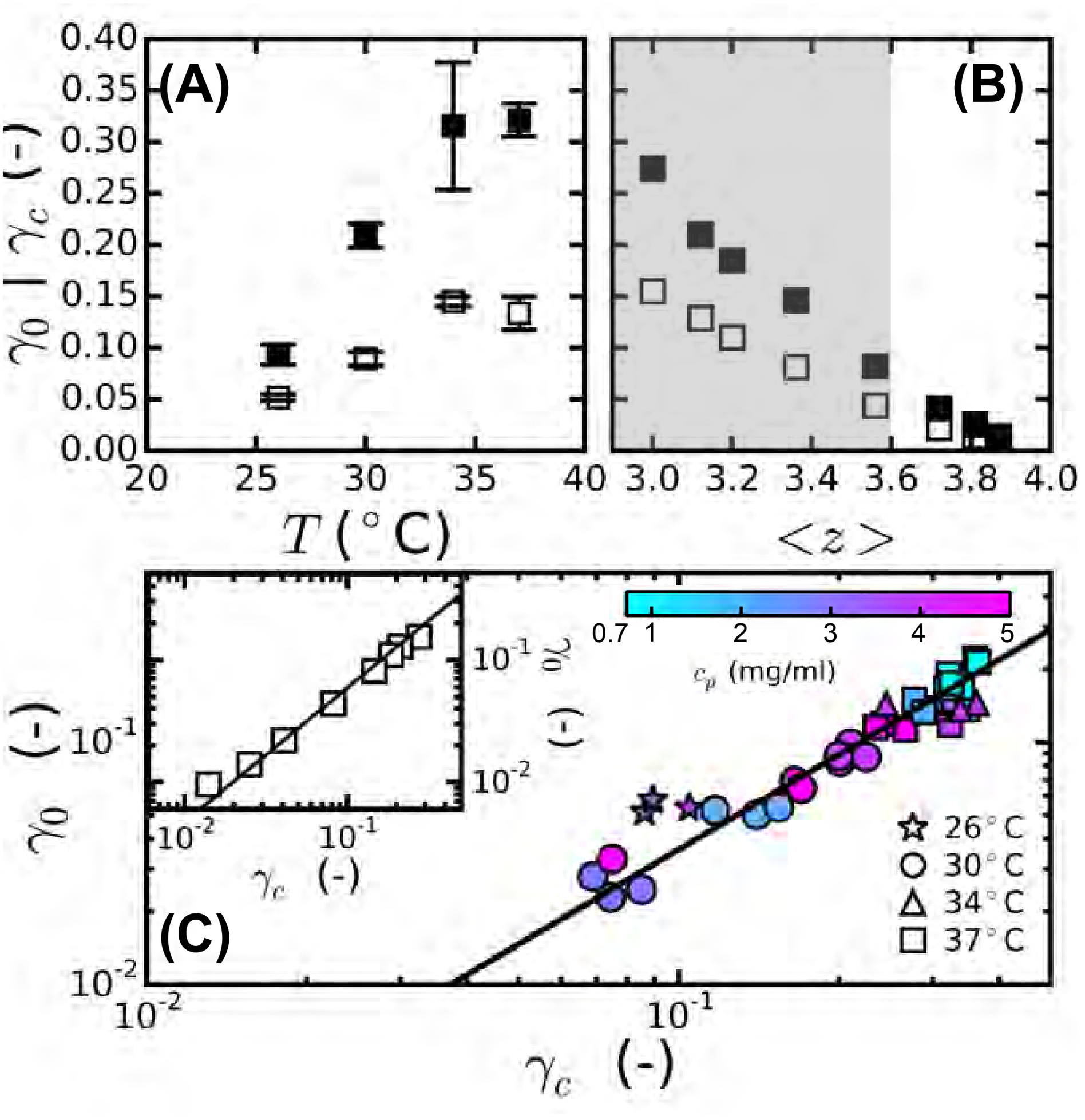
(A)
(B)
(C)
γ_0 | γ_c (-)
T (°C)
$\langle z \rangle$
γ_0 (-)
γ_c (-)
c_p (mg/ml)
26° C
30° C
34° C
37° C

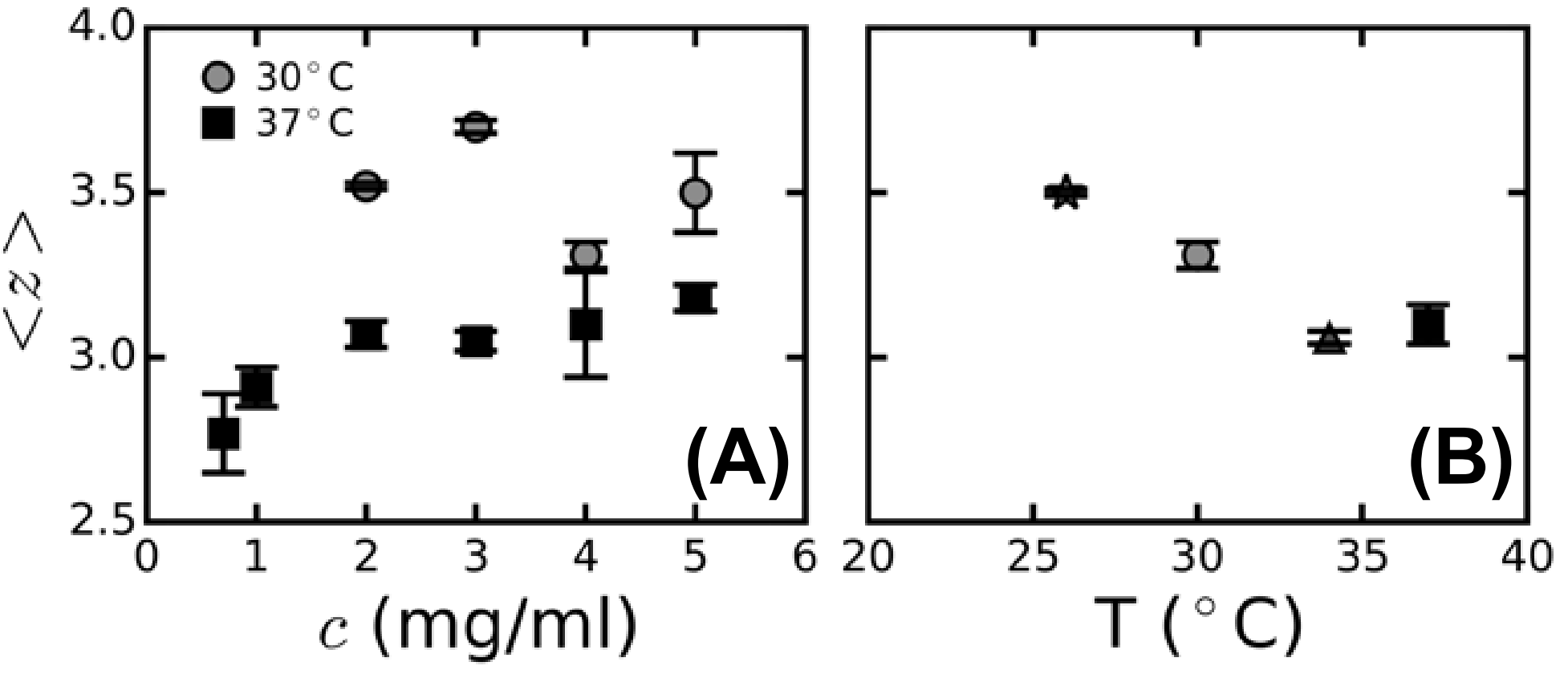
4.0
3.5
3.0
2.5
$\langle z \rangle$
30° C
37° C
(A)
0
1
2
3
4
5
6
c (mg/ml)
(B)
20
25
30
35
40
T (° C)

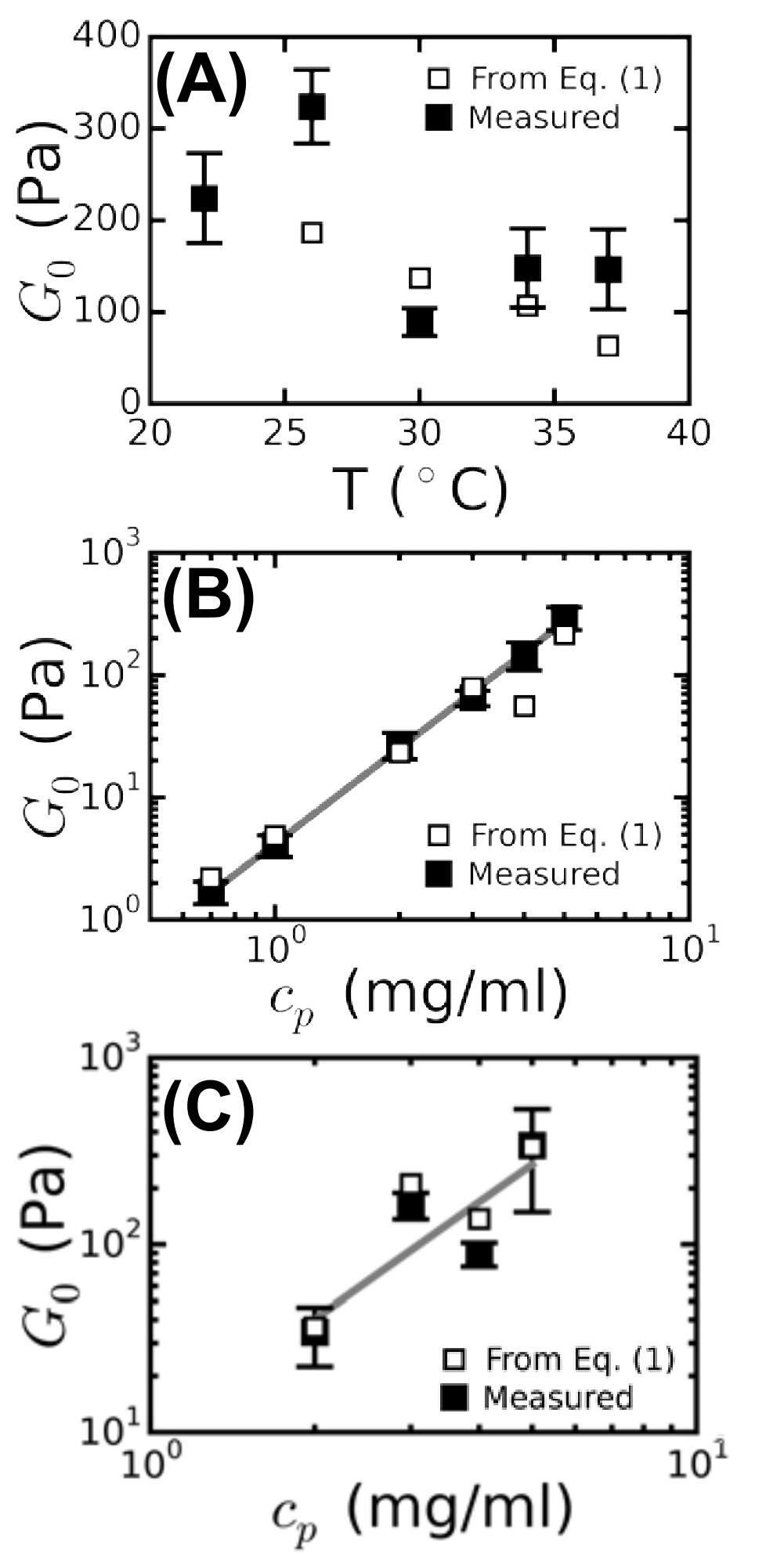
(A)
From Eq. (1)
Measured
G_0 (Pa)
T ($^\circ$C)
(B)
From Eq. (1)
Measured
G_0 (Pa)
c_p (mg/ml)
(C)
From Eq. (1)
Measured
G_0 (Pa)
c_p (mg/ml)

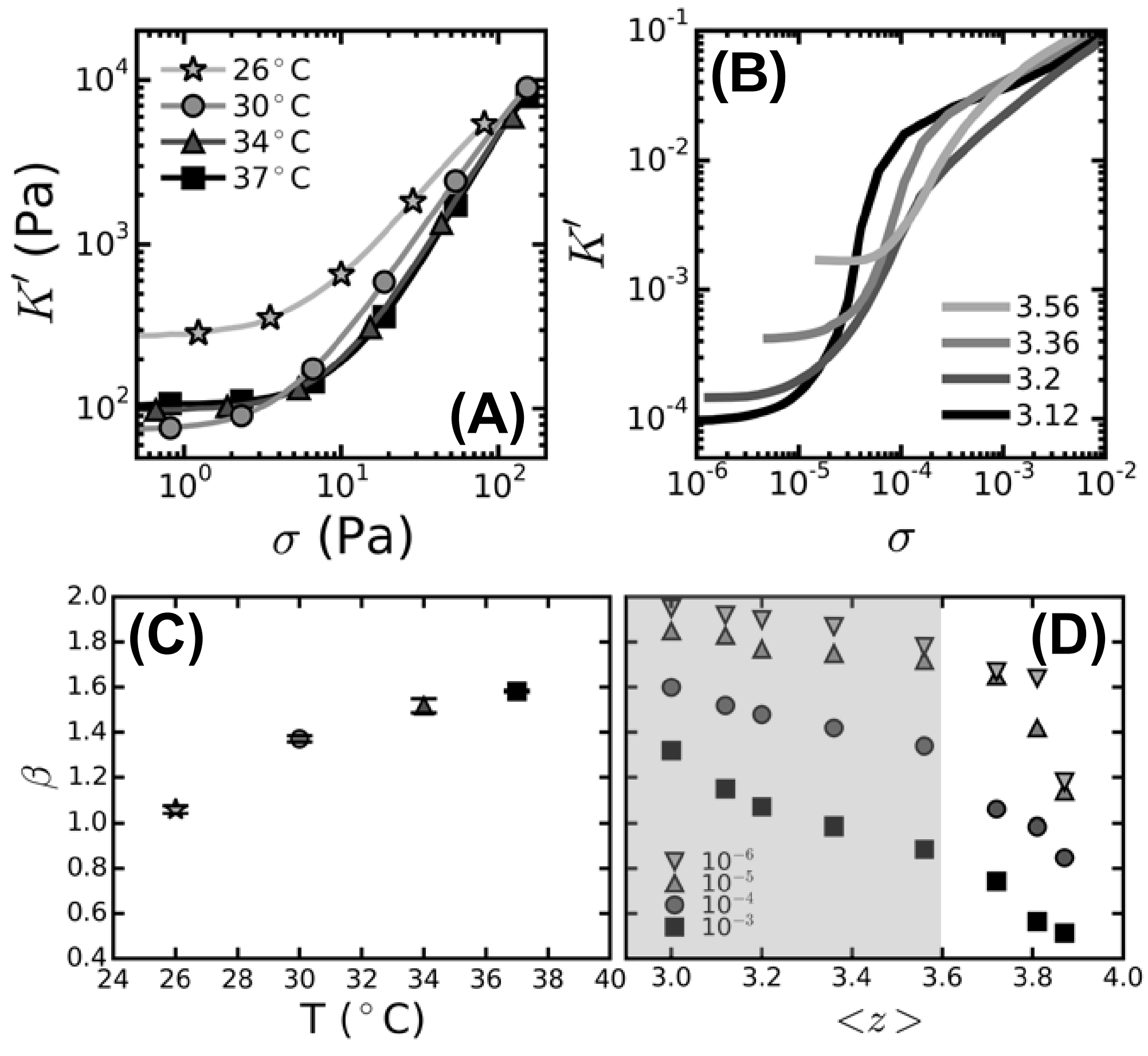
(A)
26°C
30°C
34°C
37°C
K' (Pa)
σ (Pa)
(B)
3.56
3.36
3.2
3.12
K'
σ
(C)
β
T (°C)
(D)
10^{-6}
10^{-5}
10^{-4}
10^{-3}
$\langle z \rangle$

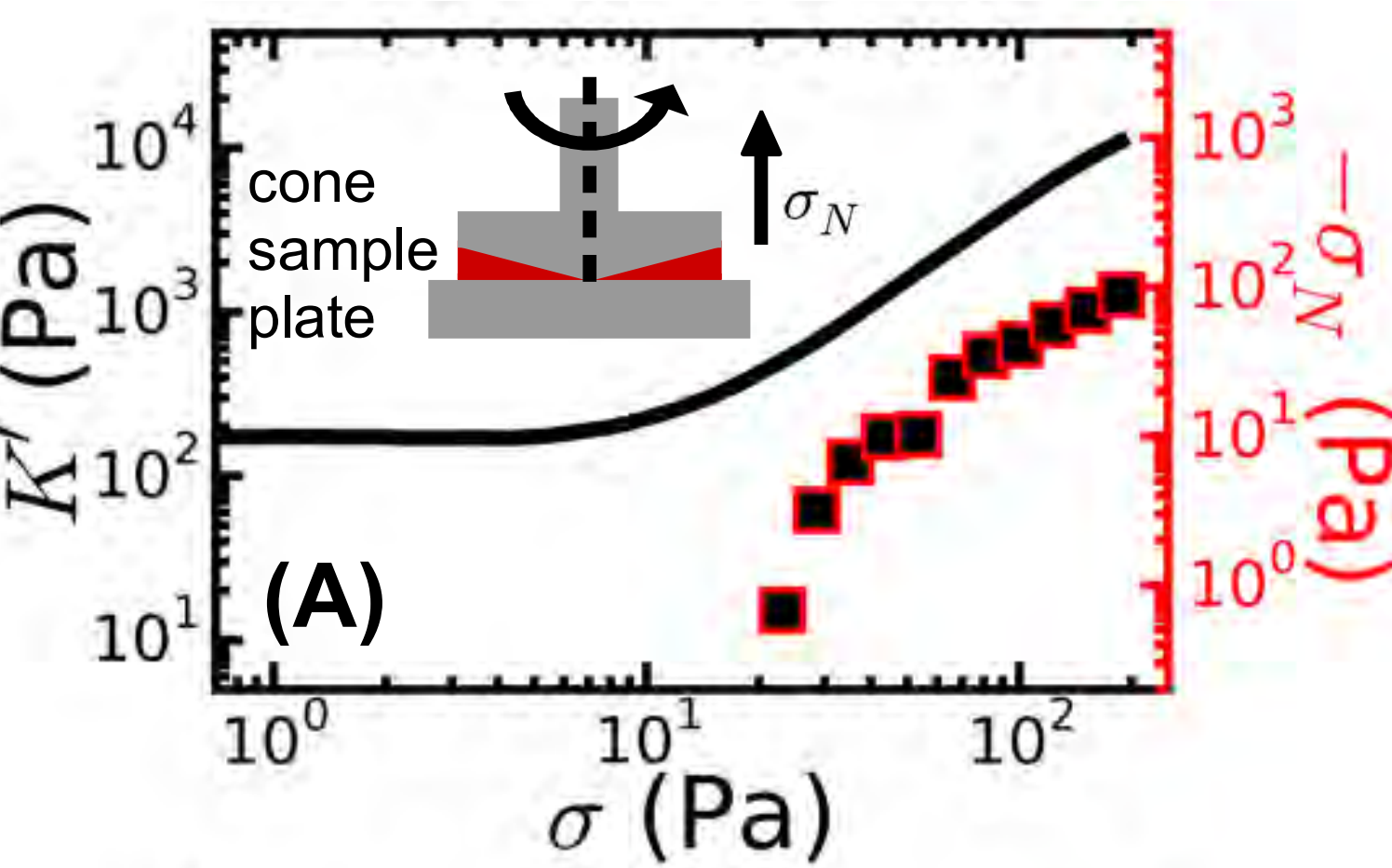
cone
sample
plate
σ_N
(A)
10^4
10^3
10^2
10^1
K' (Pa)
10^3
10^2
10^1
10^0
$-\sigma_N$ (Pa)
10^0
10^1
10^2
σ (Pa)

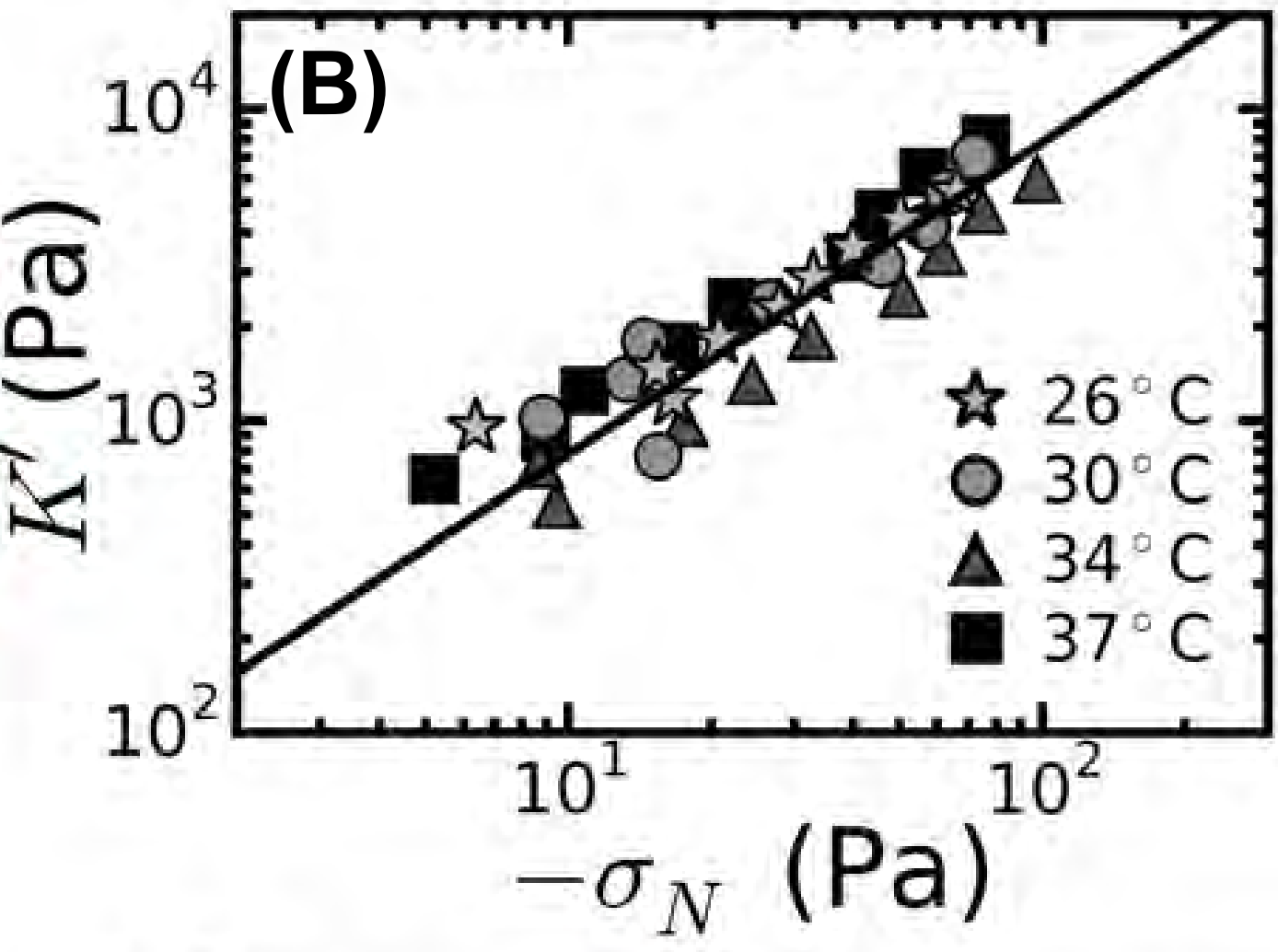
(B)
10^4
10^3
10^2
K' (Pa)
26° C
30° C
34° C
37° C
10^1
10^2
$-\sigma_N$ (Pa)

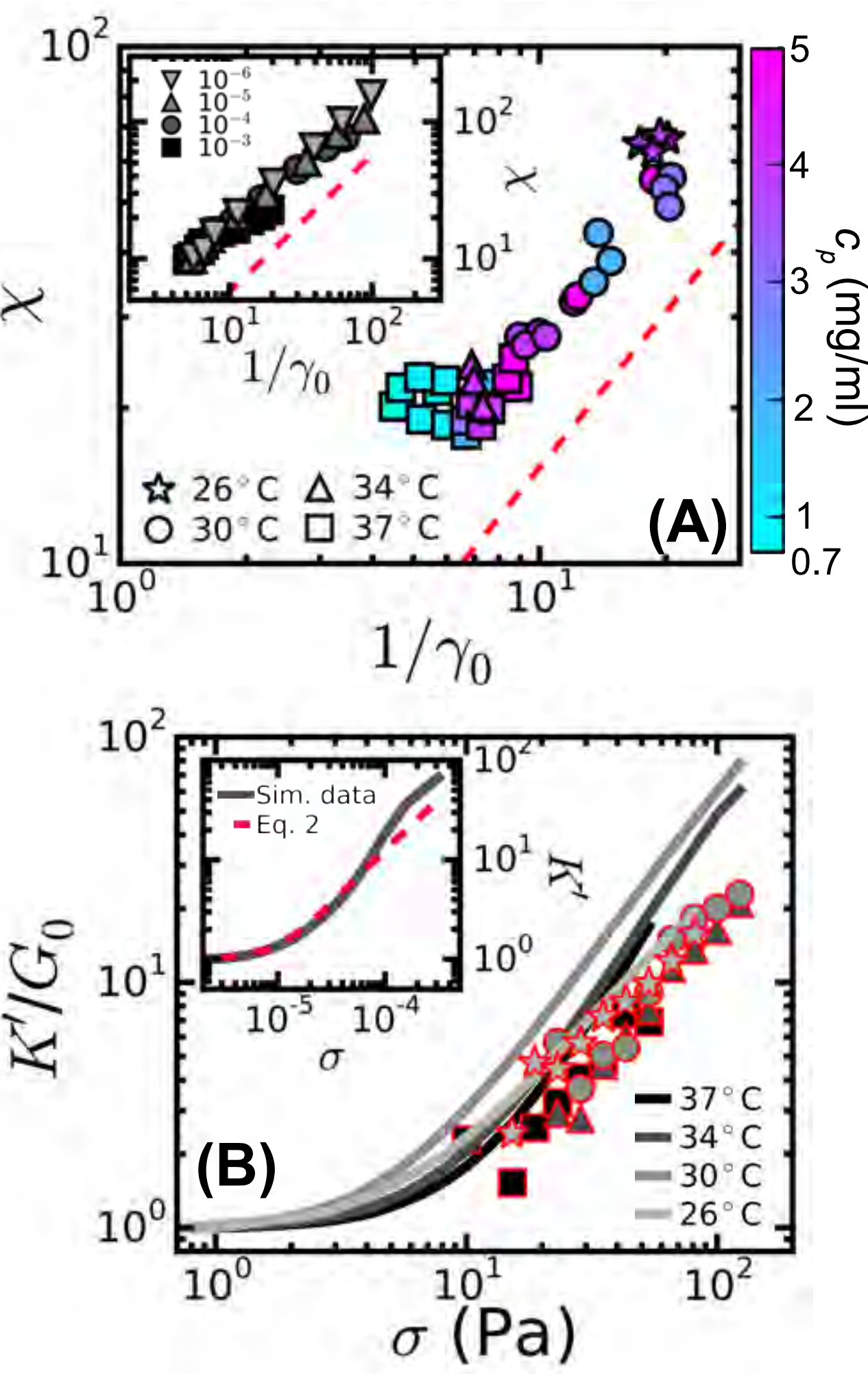
10^{-6}
10^{-5}
10^{-4}
10^{-3}
χ
$1/\gamma_0$
26° C
34° C
30° C
37° C
(A)
c_p (mg/ml)
0.7
1
2
3
4
5
Sim. data
Eq. 2
σ
K'
K'/G_0
37° C
34° C
30° C
26° C
(B)
σ (Pa)

The Role of Network Architecture in Collagen Mechanics: Supplementary Information

K.A. Jansen[1,2], A. J. Licup[3], A. Sharma[3,4], R. Rens[3], F.C. MacKintosh[3,5,6,*], G.H. Koenderink[1,*]

[1]AMOLF, Biological Soft Matter group, Science Park 104, 1098 XG Amsterdam, The Netherlands. [2]UMC Utrecht, Department of Pathology, Universiteitsweg 100, Stratenum 2.118, 3584 CG Utrecht, The Netherlands. [3]Department of Physics and Astronomy, Vrije Universiteit, 1081 HV Amsterdam, The Netherlands. [4] Leibniz-Institut für Polymerforschung Dresden, 01069 Germany. [5] Departments of Chemical & Biomolecular Engineering, Chemistry, and Physics & Astronomy, Rice University, Houston, TX 77005, USA. [6] Center for Theoretical Biophysics, Rice University, Houston, TX 77030, USA

1 Materials and Methods

1.1 Collagen network reconstitution

We polymerized acid-soluble rat tail collagen type I with intact telopeptides (high concentration stock in 0.02 N acetic acid, BD Biosciences, Breda) under physiologically relevant solution conditions that are compatible with *in vitro* cell culture. Cell culture medium (DMEM10x without phenol red), antibiotics (penicillin/streptomycin), sodium bicarbonate (7.5% sterile solution) and HEPES (2-[4-(2-hydroxyethyl)piperazin-1-yl]ethanesulfonic acid) buffer were obtained from Sigma. Chemicals were stored at 4°C, except for the antibiotics, which were stored in aliquots at -20°C. Fetal bovine serum (FBS) was obtained from Gibco and stored in aliquots at -20°C. Sterile single-use aliquots of DMEM10x, antibiotics and FBS solutions were used within 1 day.

Collagen samples were prepared by mixing all components on ice. First, collagen solution was pipetted into a precooled 2 ml Eppendorf tube. In view of the high viscosity of the collagen stock, we double-checked the accuracy of pipetting by weighing. Next, the solution ingredients were added in the following sequence: DMEM10x, HEPES, antibiotics, FBS, sodium bicarbonate and sterile milliQ water. The final solution conditions are: DMEM 1x, 1% FBS, 50 mM HEPES, 1.5 mg/ml sodium bicarbonate and 0.1% antibiotics. The pH was measured with a pH meter equipped with a micro-electrode (Hanna Instruments, Germany) and adjusted to $7.3-7.4$ with NaOH. We fixed the time between pH adjustment and insertion of the sample in the rheometer or in microscopy sample holders (glass flow chambers or glass-bottom petri dishes) to 10 min, in order to minimize potential variations due to premature polymerization on ice (1). Air bubbles were removed by centrifuging the samples before polymerization (10 s at room temperature for $2-4$ mg/ml collagen samples or several minutes at 4°C for ≥ 5 mg/ml samples). Eppendorf tubes used for preparing samples for electron microscopy (EM) were precooled on ice and rapidly warmed to the desired polymerization temperature once the sample was inserted. The rheometer bottom plate was preheated to the desired polymerization temperature before the sample was inserted. For confocal microscopy, the microscope sample chambers were filled on ice, then rapidly heated to the desired temperature after sample insertion and closure with VALAP sealant (vaseline/lanolin/paraffin in equal weights). For rheology and EM, the collagen gels were polymerized in a humid atmosphere to prevent solvent evaporation.

The polymerization temperature was varied between 22 and 37°C, while the collagen concentration was varied between 0.7 and 5 mg/ml. We chose 0.7 mg/ml as the lowest concentration, because confocal imaging revealed that networks formed at concentrations below 0.7 mg/ml exhibited dangling ends (Fig. S10 in the SI). We note that this sample preparation protocol (which is widely used in *in vitro* studies of collagen and of cell-seeded collagen gels) results in a variation of the acetic acid content and the serum-to-collagen ratio with collagen concentration. This may potentially contribute to the variation in $\langle z \rangle$ we observe with collagen concentration at 37°C, although we favor the interpretation that $\langle z \rangle$ is below 3 at collagen concentrations of 1 mg/ml and below due to the presence of dangling fiber ends.

1.2 Collagen network rheology

Rheology tests were performed with a stress-controlled rheometer (Physica MCR 501, Anton Paar, Graz, Austria) using a stainless steel cone-plate geometry with 40 mm diameter and 1° cone angle. Measurements using a 40 mm cone-plate with 2° cone angle of either polycarbonate or stainless steel gave similar results (*data not shown*). Neutralized cold collagen solution was pipetted onto the plate and the cone was immediately lowered. The sample was trimmed while keeping the angular position of the cone fixed. A solvent trap was added to prevent solvent evaporation. Collagen networks were allowed to form undisturbed (without mechanical probing) for 6 hours. We double-checked by turbidity measurements that even at 22°C, where polymerization is known to be rather slow (2–4), the networks were fully formed after ∼200 minutes (*data not shown*).

Once each network was formed, we probed its linear viscoelastic behavior by applying oscillatory shear with a small (0.5%) strain amplitude and frequencies ranging from 10 to 0.05 Hz. Next, a prestress protocol was performed to determine the nonlinear mechanical properties. We applied a stepwise increasing level of constant shear stress, σ, and measured first the resulting strain γ for 30 s (*creep test*). During this creep test, the normal force build-up was recorded and the final force level is reported. Next the differential viscoelastic moduli were measured by superposing 6 consecutive oscillations with a frequency of 0.5 Hz and an amplitude $\delta\sigma = 0.1\sigma$ (*prestress test*). Per shear stress decade, 11 data sets were collected, equally spaced on a logarithmic scale. From the prestress tests, we extracted the differential modulus, $K^* = \delta\sigma/\delta\gamma$, as the ratio between the applied oscillatory stress $\delta\sigma$ and the resulting oscillatory strain response $\delta\gamma$, taking an average over the last 5 oscillations. $K^* = K' + K''$ has an elastic component K' and a viscous component K''. We defined the onset stress, σ_0 (and corresponding onset strain, γ_0) for strain-stiffening as the stress where K'/σ versus σ has a local minimum (see Fig. S5 in the SI) and the critical strain, γ_c, as the inflection point of $\log(K'(\gamma))$ curves in the nonlinear regime (see Fig. S6 in the SI). We furthermore characterized stress-stiffening by the stiffening exponent β, which was defined as the maximal power law slope of strain-stiffening curves (obtained by taking the first derivative of K' versus σ_0).

We note that in this paper we consider only the elastic response of the collagen networks. To test the importance of the viscous response, we probed the elastic and viscous moduli over a range of frequencies between 0.05 and 10 Hz by applying a small amplitude oscillatory strain deformation with an amplitude of 0.5%. As shown in Figure S11(A), the networks behave as soft viscoelastic solids with an elastic shear modulus (G') that is at least 5-fold larger than the viscous shear modulus (G'') across the entire frequency range. As shown in the inset, the loss tangent, $\tan(\delta) = G''/G'$, remains well below 0.2 at all temperatures. The loss tangent slightly decreases with increasing collagen concentration, going from 0.2 at 0.5 mg/ml to 0.1 at 5 mg/ml (Fig. S11B). These observations are in line with previous reports (5, 6). We conclude that the networks studied in this paper are indeed predominantly elastic.

All rheological data shown are averages ± standard deviation for 3 independently prepared samples, unless stated otherwise. Errors in best-fit values are expressed as the standard error, unless stated otherwise.

2 Turbidity measurements of collagen fibril thickness

Turbidity measurements were performed using a Cary300 UV-Vis spectrophotometer (Agilent Technologies, Amstelveen, Netherlands). Collagen network formation was allowed to run to completion in plastic cuvettes (UV-Cuvette micro, Plastibrand, Germany) by incubating for at least 6 hours and at most overnight at temperatures between 22 and 37°C. Optical density measurements were performed over a range of wavelengths λ of 350−900 nm. The turbidity τ follows from the transmitted intensity I_0 as:

$$\tau = \frac{I_0 \ln(10)}{L} \tag{1}$$

where *L* is the optical path length. Assuming that the collagen fibers can be modeled as randomly oriented, monodisperse rod-like particles with a small radius and long length compared to λ, the turbidity measurements can be rescaled to reveal the average mass-length ratio μ and the radius a of the fibers (7–9):

$$\tau\lambda^5 = A\mu(\lambda^2 - Ba^2), \tag{2}$$

where $A = (88/15)c_p\pi^3 n_s(dn/dc_p)^2/N_A$ and $B = (184/154)\pi^2 n_s^2$ are constants. Here c_p is the collagen mass concentration in *g/ml*, n_s is the solvent refractive index (1.33), dn/dc_p is the specific refractive index increment (0.186 cm^3/g for collagen (10)), and N_A is Avogadro's constant. We included a correction factor for wavelength dispersion in the solvent and the differential refractive index (9). We fitted the data between wavelengths of 890 and 650 nm, to ensure that the OD did not exceed the maximum measurable OD of 2.8 at the smallest λ and was above the noise floor at the highest λ. The average number of monomers per cross-section, N, was determined from μ based on the known quarter-staggered molecular packing structure of the fibrils and the molecular mass of a collagen monomer (290 kDa (11)):

$$N = \frac{4.6D \cdot \mu}{M} \tag{3}$$

where *D* is the axial (D-banding) periodicity (67.2 nm).

All turbidity data shown are averages $\pm$ standard deviation for a minimum of 3 independently prepared samples. Errors in best-fit values are expressed as the standard error, unless stated otherwise.

3 Collagen network imaging

Label-free imaging of collagen networks in the native, hydrated state was performed by confocal reflectance microscopy with an inverted Eclipse Ti microscope (Nikon), using an 488 Ar laser (Melles Griot, Albuquerque, NM) for illumination. Confocal slices were recorded over a total z-distance of 20 μm (using a 100x N.A. 1.49 objective) or 40 μm (using a 40x N.A. 1.30 objective) with a step size of 0.2 μm and starting at least 10 μm away from the coverslip surface. For display purposes, the confocal z-stacks were summed to give an impression of the typical mesh size of the networks and the degree of spatial (in)homogeneity. Statistics: nr of samples, nr of fields of view

For scanning electron microscopy (SEM), 4 mg/ml collagen gels (50-100 μl sample volume) were polymerized overnight in Eppendorf tubes maintained at different temperatures ($22 - 37\,^{\circ}\mathrm{C}$) using a water bath. After polymerization, the samples were prepared for SEM using a protocol adapted after Refs. (12, 13). The samples were first washed three times in sodium cacodylate buffer (50 mM cacodylate, 150 mM NaCl, pH 7.4) for $30-60$ min at their original polymerization temperature, to prevent depolymerization (14). The samples were fixed with 2.5% glutaraldehyde in the same buffer for at least 2 hours. Next, the samples were washed three times with sodium cacodylate buffer (room temperature) and dehydrated in ethanol/ milliQ water while increasing the volume percentage of ethanol stepwise, from 30 to 50, 70, 80, 90, 95, and finally 3 times 100%. Next, the samples were washed twice with 50% hexamethyldisilazane (HMDS) in ethanol for 30 min in a fume hood, and incubated for 30 min in 100% HMDS. Finally, the samples were air-dried overnight in the fume hood, transported to a stub with carbon tape, and coated with a 15.4 nm layer of Au/Pd using a K575X sputter coater at a current of 80 mA (Quorum Technologies, Gouda, The Netherlands). The samples were imaged with a STEM microscope (Verios 460, FEI Company, Eindhoven, the Netherlands) in immersion mode using a current of 50 pA, voltage of 5 kV, and 4 mm working distance.

The diameter of the collagen fibrils was measured manually from SEM images obtained for 4 samples at each condition, and at magnifications between 10000 and 50000. Fibers were selected at random by overlaying a grid of crosses on the images using the Grid-plugin in Fiji spaced by 1.5 μm. Cross-sectional widths of fibers at the crosses were measured and per sample at least 250 fibers were included in the analysis. The average connectivity $\langle z \rangle$ of the networks was extracted from the images by subdividing the SEM images taken at magnifications in the range of 20,000 to 50,000 into 5x5 squares. In every other square, we counted the number of fibers at each junction that was in the focal plane. We analyzed more than 100 junctions per sample, with 4 samples taken at $T = 26^{\circ}$C and 3 samples at $T = 30^{\circ}$C, 34°C, and 37°C. We were unable to determine the fiber diameter or $\langle z \rangle$ values for $T = 22^{\circ}$C collagen networks due to the inhomogeneous structure of the fan-shaped bundles and of the network as a whole.

4 Computational Model of Collagen Network Rheology

4.1 Simulating Submarginal Networks

We model collagen networks as disordered lattice-based structures. Lattice models have the advantage that they are computationally inexpensive and the network connectivity can be easily varied. The primary determinant of the elastic properties of collagen networks is the local connectivity because collagen networks have a connectivity that is below the Maxwell isostatic stability limit for networks of Hookean springs (15). The Maxwell criterion for mechanical stability of spring networks requires a mimimum connectivity of $z_{crit} = 2d$, where d is the dimensionality (16). At the isostatic (or marginal) point, corresponding to $z = 6$ in 3D, the number of degrees of freedom is just balanced by the number of constraints. Collagen networks have a typical average connectivity between 3 (due to fiber branches) and 4 (from binary crosslinks) (15, 17, 18), placing them well below this threshold. Collagen networks nevertheless exhibit a finite elasticity as a result of the large bending rigidity of the fibers (19). There is already evidence that disordered lattice models can capture the elastic properties of collagen networks prepared under specific conditions well (15, 18, 20).

Here we focus primarily on 2D triangular lattices, described in detail elsewhere (15, 18, 20). These lattices have a spacing l_c and dimensions WxW, where $W = 50l_c$. We enforce local 4-fold connectivity by a phantomization procedure, where a binary cross-link is formed between two randomly selected fibers at each vertex while treating the third fiber as a phantom that does not interact with the other two fibers. Next we reduce $\langle z \rangle$ to a value between 3 and 4 by bond dilution, which

involves random removal of segments with a probability q. This procedure reduces the average fiber length to $L = l_c/q$. Thus, the networks are, by construction, sub-isostatic and floppy in the absence of bending interactions. Each filament is assigned a stretching modulus, μ_s, and a bending modulus, κ. These two parameters define a dimensionless measure of the relative bend-stretch stiffness:

$$\widetilde{\kappa} = \kappa/\mu_s l_c^2 \tag{4}$$

Treating collagen fibers as homogeneous elastic beams with a cylindrical cross-section, $\mu_s = \pi a^2 E$, and $\kappa = \frac{1}{4}\pi a^4 E$ (21). Here, a is the fibril radius and E is the Young's modulus. Thus, $\tilde{\kappa}$ can be rewritten as:

$$\tilde{\kappa} = \frac{\frac{\pi}{4}a^4 E}{(\pi a^2 E) l_c^2} = \frac{1}{4}\frac{a^2}{l_c^2}. \tag{5}$$

Note that $\widetilde{\kappa}$ is determined solely by the geometrical parameters a and l_c, while being independent of the material properties of the fibers.

The lattices are subjected to a simple shear strain, γ, and allowed to relax by minimization of the total elastic energy per unit volume, H, which is calculated according to a discrete form of the extensible wormlike chain Hamiltonian:

$$\mathcal{H} \simeq \sum_{f=1}^{N}\left[\frac{\mu}{2}\sum_{\langle ij\rangle\in f}\ell_0\left(\frac{\delta\ell_{ij}}{\ell_0}\right)^2 + \frac{\kappa}{2}\sum_{\langle ijk\rangle\in f}\ell_0\left\|\frac{\hat{t}_{jk}-\hat{t}_{ij}}{\ell_0}\right\|^2\right] \tag{6}$$

The stress follows from the minimum energy as: $\sigma = dH/d\gamma$, while the differential elastic shear modulus follows as: $K = d^2H/d\gamma^2$. Stress and stiffness are measured in units of μ/l_c^{d-1}, where d is the dimensionality.

4.2 Estimation of G_0 of collagen networks

In order to directly compare the measured elastic linear modulus of collagen networks with predictions of the model, we express G_0 in terms of experimentally measurable parameters, in particular volume fraction φ and average connectivity $\langle z\rangle$. From the model described in more detail in (20), G_0 is proportional to the fiber stretching modulus μ_s, line density ρ, and reduced fiber rigidity $\tilde{\kappa}$:

$$G_0 = A\mu_s\rho\tilde{\kappa}\left(\frac{L}{l_c}\right)^{2/\zeta}, \tag{7}$$

where A is a prefactor that depends on local network geometry through $\langle z\rangle$, and ζ is a dimensionless exponent equal to 1 for 2D and 3D lattice-based random networks. Assuming the network is made up of N such rods of length L randomly arranged in a total volume V, the line density can be defined as $\rho = \frac{NL}{V}$. The rods occupy a total volume $\pi a^2 NL$ and the volume fraction φ is therefore

$$\varphi = \frac{\pi a^2 NL}{V} = \pi a^2\rho. \tag{8}$$

Substituting μ_s and ρ from (8) back in (7) gives:

$$G_0 = A\tilde{\kappa}\left(\frac{L}{l_c}\right)^2 E\varphi. \tag{9}$$

We can obtain the line density for diluted 3D phantom fcc lattices by considering that there are $6p$ intersecting fibers at every vertex and p is the probability that a lattice bond of length l_c is connected to that vertex. We enclose any vertex by a sphere of radius $l_c/2$. The total length of fibers within the sphere must be $6pl_c$. Dividing this length by the volume of the enclosing sphere, we obtain the line density of the 3D fcc lattice:

$$\rho_{3D} = \frac{6pl_c}{\frac{4}{3}\pi\left(\frac{l_c}{2}\right)^3}\left(\frac{\pi}{\sqrt{18}}\right) = \frac{\tilde{\rho}_{3D}}{l_c^2}, \tag{10}$$

where $\tilde{\rho}_{3D} = \frac{12p}{\sqrt{2}}$. We have multiplied the line density by $\frac{\pi}{\sqrt{18}}$ to account for maximal spherical packing within the fcc lattice. Substituting (10) for ρ in (8) and using (5), we obtain:

$$\varphi = \pi a^2 \frac{\tilde{\rho}_{3D}}{l_c^2} = 4\pi \tilde{\rho}_{3D} \tilde{\kappa} = \frac{48\pi p}{\sqrt{2}} \tilde{\kappa} \approx \frac{12\pi z}{\sqrt{2}} \tilde{\kappa}. \tag{11}$$

The last expression uses the approximate relation $z \approx 4p$. We can finally substitute $\tilde{\kappa}$ from (11) back to (9) to get:

$$G_0 = F(z) E \varphi^2, \tag{12}$$

where:

$$F(z) \simeq \frac{A\sqrt{2}}{12\pi z} \left(\frac{L}{l_c} \right)^2 \tag{13}$$

A is a constant equal to 1.5 ± 0.3 (22). Values of $F(z)$ are given for 3D networks of varying $\langle z \rangle$ and L/l_c in Table S1.

5 Supplementary Figures

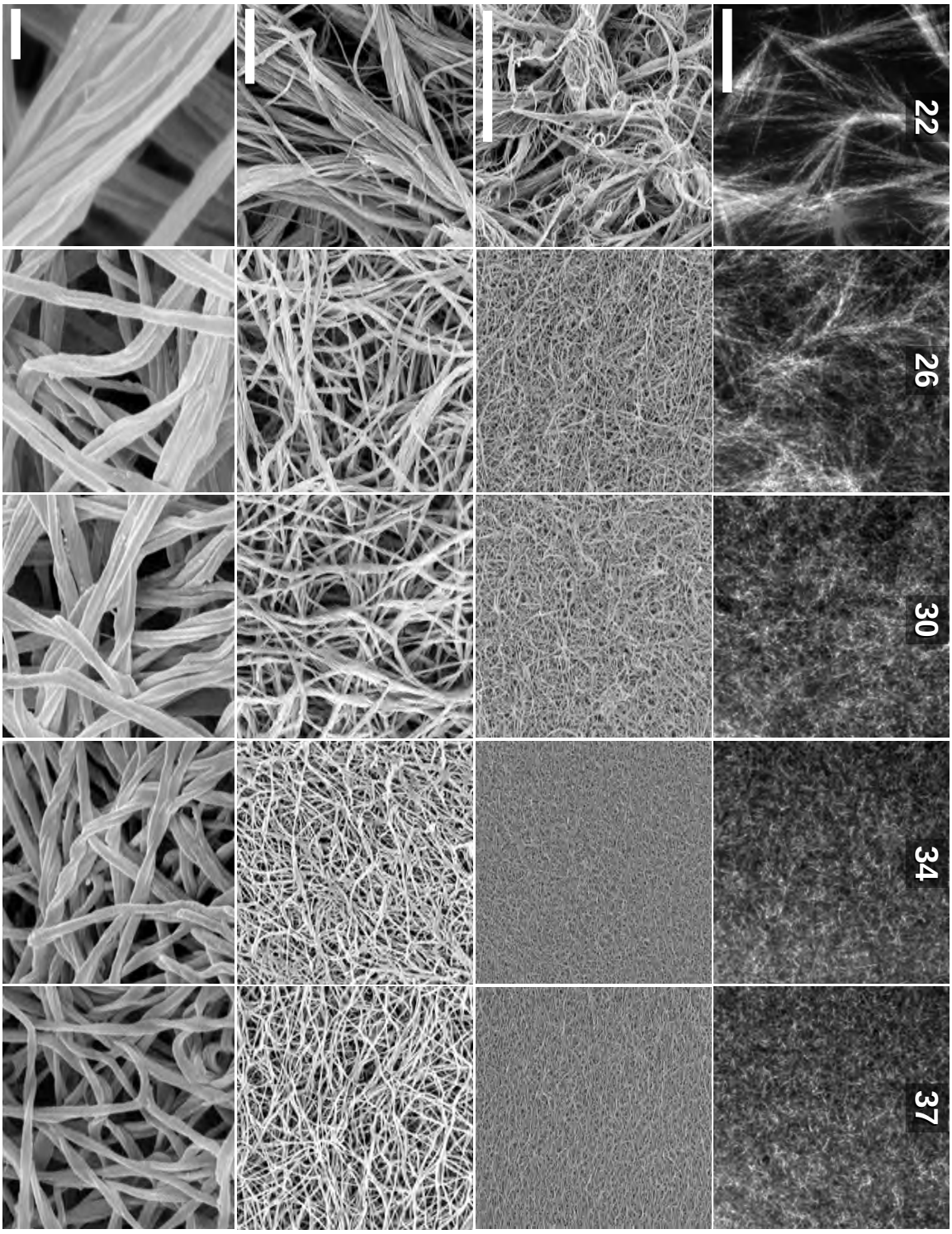

Figure S1: Temperature dependence of the microstructure of 4 mg/ml collagen networks observed at different magnifications, and comparing confocal imaging of hydrated samples with SEM imaging of dried samples (rotated). The polymerization temperature is indicated above each column in units of °C. *(row 1)* Confocal reflection images, showing an open network of 'fan-shaped' fibril bundles at 22 °C and progressively more homogeneous and dense networks with increasing temperature. Scale bar: 20 μm. *(row 2-4)* Scanning Electron Microscopy (SEM) images at three different magnifications: the scale bars denote 20 μm (row 2), 2 μm (row 3), and 200 nm (row 4).

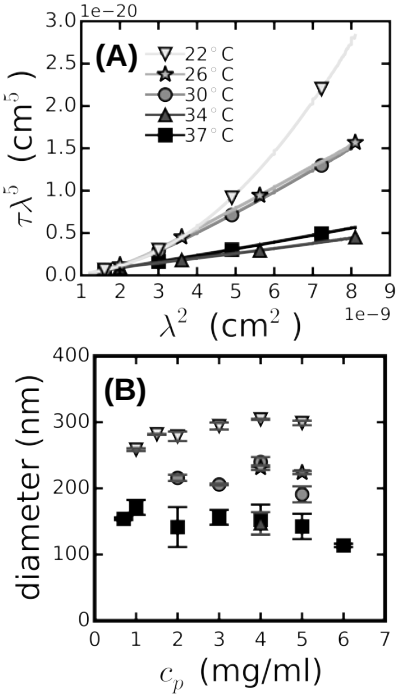

Figure S2: (A) Representative example measurements of the turbidity, τ, as a function of wavelength, λ, for 4 mg/ml collagen networks polymerized at different temperatures. The curves are rescaled according to Eq. (2) in the SI. The functional dependence is linear for networks polymerized at temperatures between 26°C and 37°C, as expected for random networks of stiff rods. The dependence is nonlinear for networks formed at 22°C, indicating a heterogeneous structure. Data points were taken with λ-increments of 2 nm and the symbols are for clarification only. Note that these curves are representative examples measured on single networks. (B) Concentration dependence of the fibril diameter for collagen networks assembled at different temperatures, as determined by turbidimetry. Gradient in symbol colors and shapes denotes polymerization temperatures of 22 (triangles down), 26 (stars), 30 (circles), 34 (triangles up) and 37°C (squares). Data points are averages $\pm$ standard deviation for a minimum of 3 samples per condition.

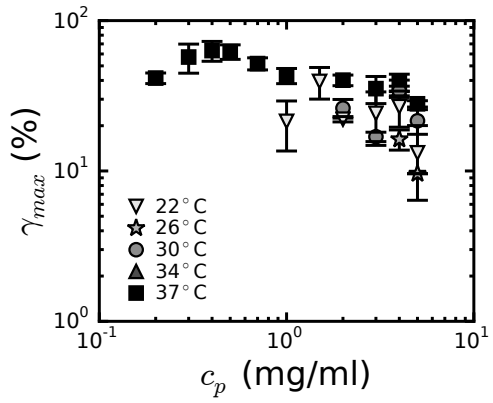

Figure S3: Concentration dependence of the maximal strain, γ_{max}, reached before the network ruptures or detaches from the rheometer plates, for collagen gels polymerized at temperatures of 22°C (triangles down), 26°C (stars), 30°C (circles), 34°C (triangles up) and 37°C (squares), in increasing shades of gray. Data points are averages $\pm$ standard deviation for 3 samples per condition.

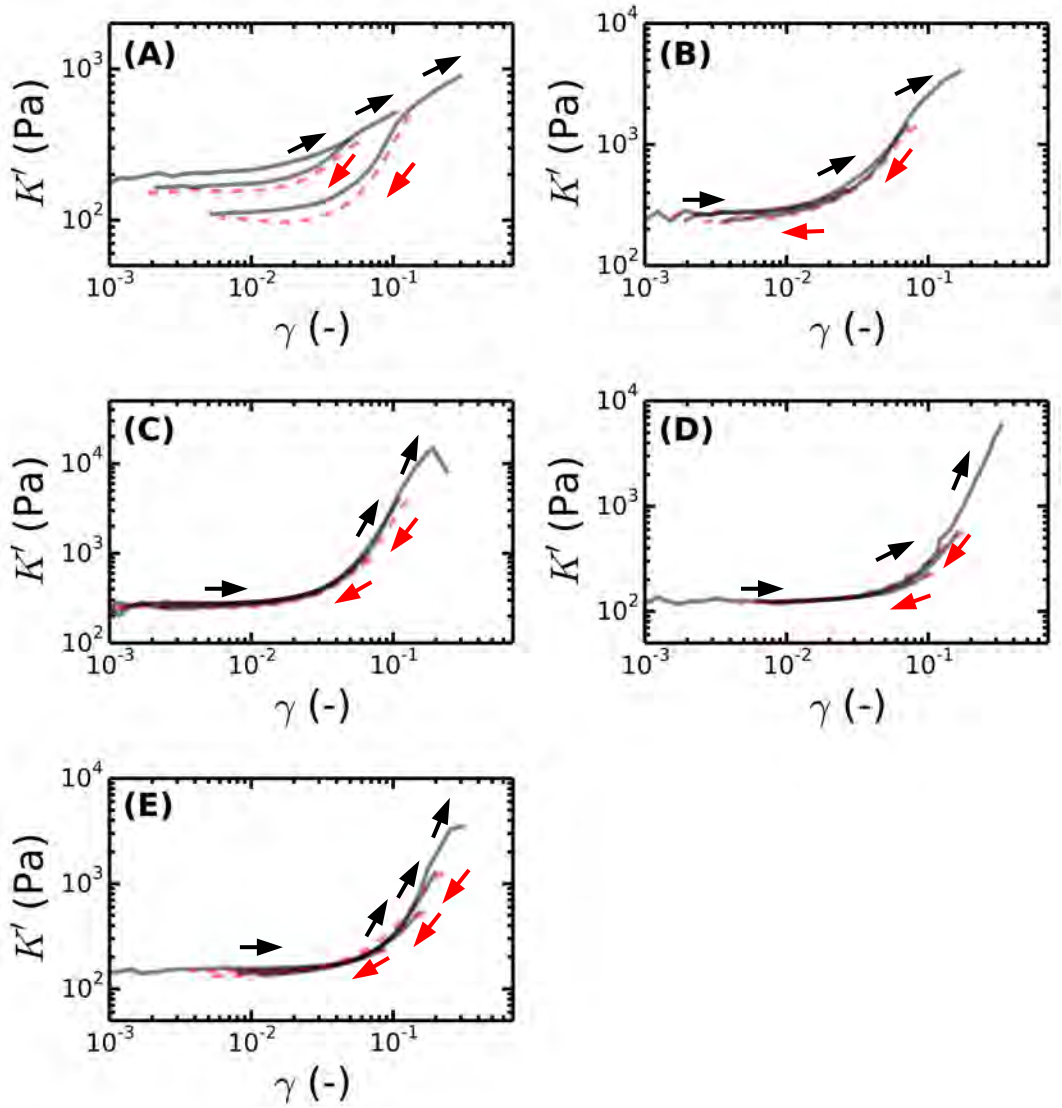

Figure S4: Hysteresis stress-ramp tests for 4 mg/ml collagen gels formed at different polymerization temperatures. The shear stress was increased up to a certain level (gray lines, black arrows) and then decreased back down to the linear regime (red dashed lines, red arrows) while recording the strain. This procedure was repeated, with progressively increasing maximum stress level. The polymerization temperature was 22°C (A), 26°C (B), 30°C (C), 34°C (D) and 37°C (E). Significant hysteresis between upward and downward stress sweeps accompanied by a progressive softening of the linear modulus upon repeated testing was observed only for networks formed at 22°C. Note that all curves shown are representative examples measured on single networks.

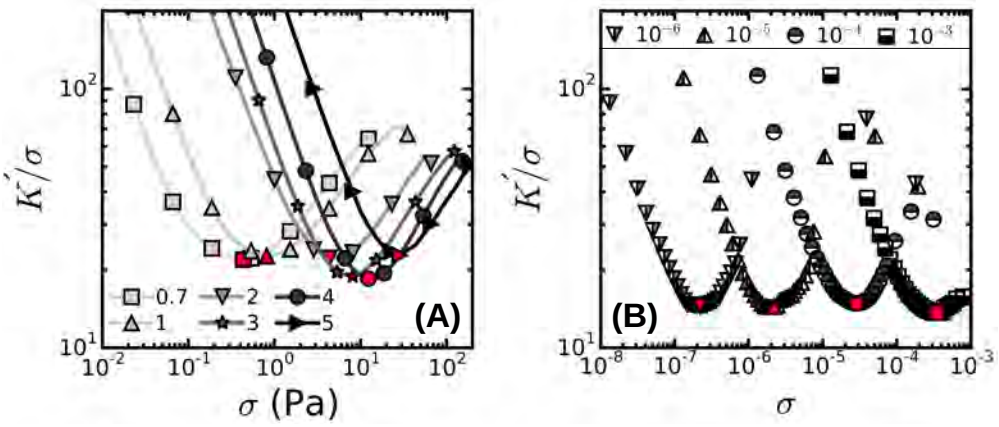

Figure S5: Definition of the onset stress where elastic nonlinearity sets in, σ_0. (A) Definition of σ_0 as the minimum of K'/σ versus σ curves, showing representative measurements on collagen networks polymerized at 37°C for collagen concentrations of 0.7 (squares), 1 (triangles up), 2 (triangles down), 3 (stars), 4 (circles) and 5 mg/ml (triangles right), in increasing shades of gray (see legend). These curves are representative examples measured on single networks. (B) We can identify σ_0 in the same fashion in simulation data for fixed $L/l_c = 3.1$ and varying dimensionless bending rigidities $\widetilde{\kappa}$: 10^{-6}, 10^{-5}, 10^{-4}, and 10^{-3} (see legend). Red symbols in (A) and (B) denote the onset of stiffening.

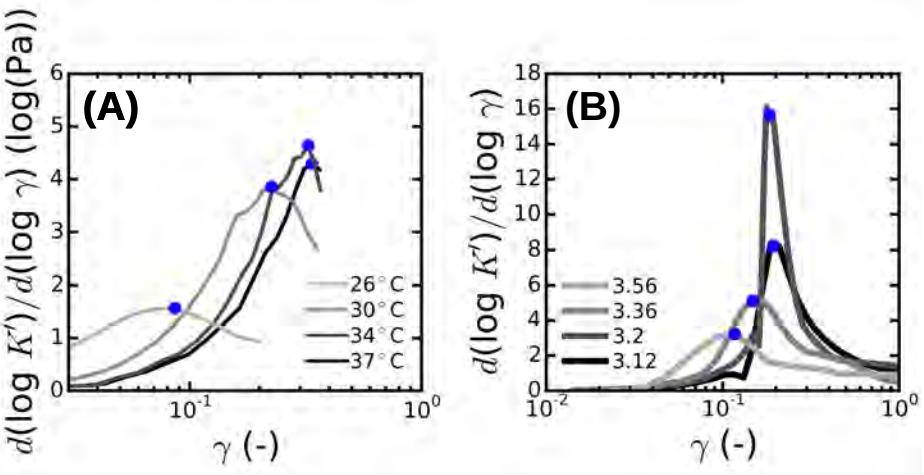

Figure S6: Definition of γ_c as the inflection point of $K'(\gamma)$ versus γ curves. These inflection points were determined by plotting the derivative of $d\log(K)/d\log\gamma$ against γ and determining the maximum (blue dots). We can define γ_c in the same fashion in simulation data of 2D fibrous networks. In (A), collagen data for 4 mg/ml are shown, where the polymerization temperature is increased from 26, 30, 34 and 37 °C in increasing shades of gray (see legend). The curves are representative examples measured on single networks. In (B), $\widetilde{\kappa}$ was held fixed at 10^{-4} and $\langle z \rangle$ was varied (data for z =3.12, 3.2, 3.36 and 3.56 are shown as indicated by the legend).

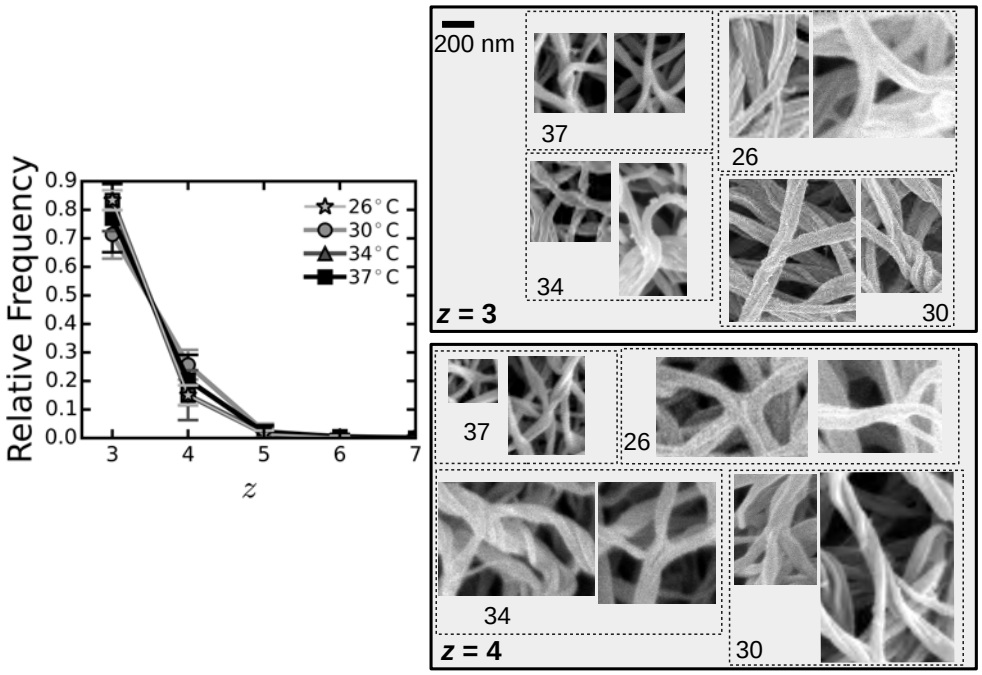

Figure S7: Histograms showing the distribution of measured local connectivities, z, obtained by randomly sampling junctions in SEM images and counting the number of fibers that meet at the junction. The gradient in symbol gray levels and shapes denote polymerization temperatures of 26 (stars), 30 (circles), 34 (triangles up) and 37°C (squares). The image gallery shows examples of $z = 3$ and $z = 4$ junctions for these temperatures. We often observe that fibers emerging from branch points have unequal diameters. Data points in the left panel are averages $\pm$ standard deviation obtained for 100 junctions per condition (from 4 samples prepared at 26°C and 3 samples at 30, 34, and 37°C.

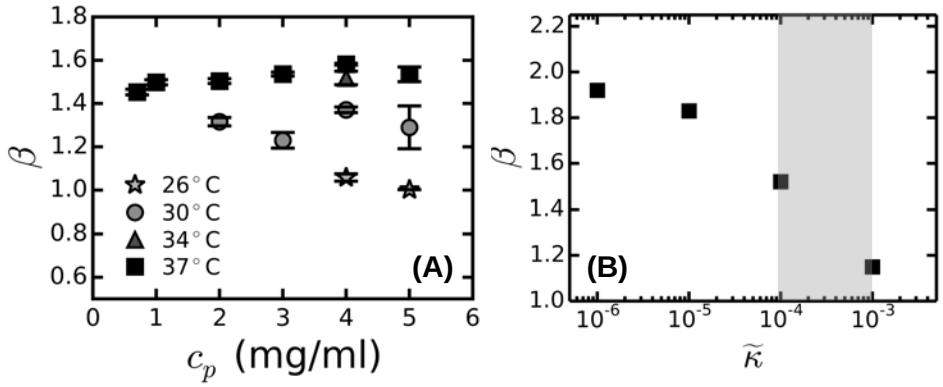

Figure S8: Comparison between the concentration dependence of the stress-stiffening exponent, β, measured for collagen networks and simulation results for the $\widetilde{\kappa}$ dependence of β. Data points are averages $\pm$ standard deviation for 3 samples per condition. In the experimentally relevant $\widetilde{\kappa}$-range (highlighted in gray in panel B), β varies over a similar range $(1.1 - 1.6)$ as in experiments. (A) Measurements on 4 mg/ml collagen gels polymerized at different temperatures denoted by symbols with an increasing gray level: 22°C (triangles down), 26°C (stars), 30°C (circles), 34°C (triangles up) and 37°C (squares). (B) Simulations reveal that β for fibrous networks decreases with increasing $\widetilde{\kappa}$ at a fixed network architecture (here $z = 3.2$).

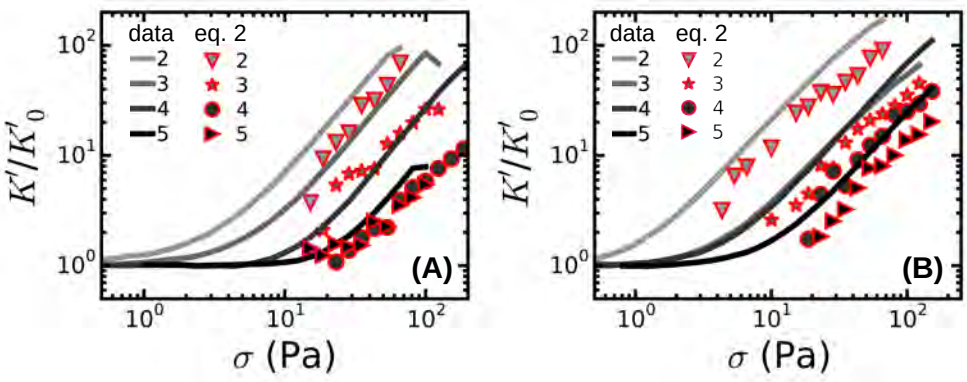

Figure S9: Concentration-dependent measurements demonstrate that the initial stress-stiffening response of collagen gels is governed by normal stress for a range of collagen networks polymerized at different concentrations and temperatures. This is shown by comparing stress-stiffening curves (lines) obtained either 37°C (A) or 30°C (B)) to predictions based on Eq. 2 in the main text (symbols), which uses measurements of the normal stress and the susceptibility as input. In both panels, the collagen concentration was 2 (triangles down), 3 (stars), 4 (circles) and 5 mg/ml (triangles right), in increasing shades of gray (see legends). Note that all data shown are representative examples measured on single networks.

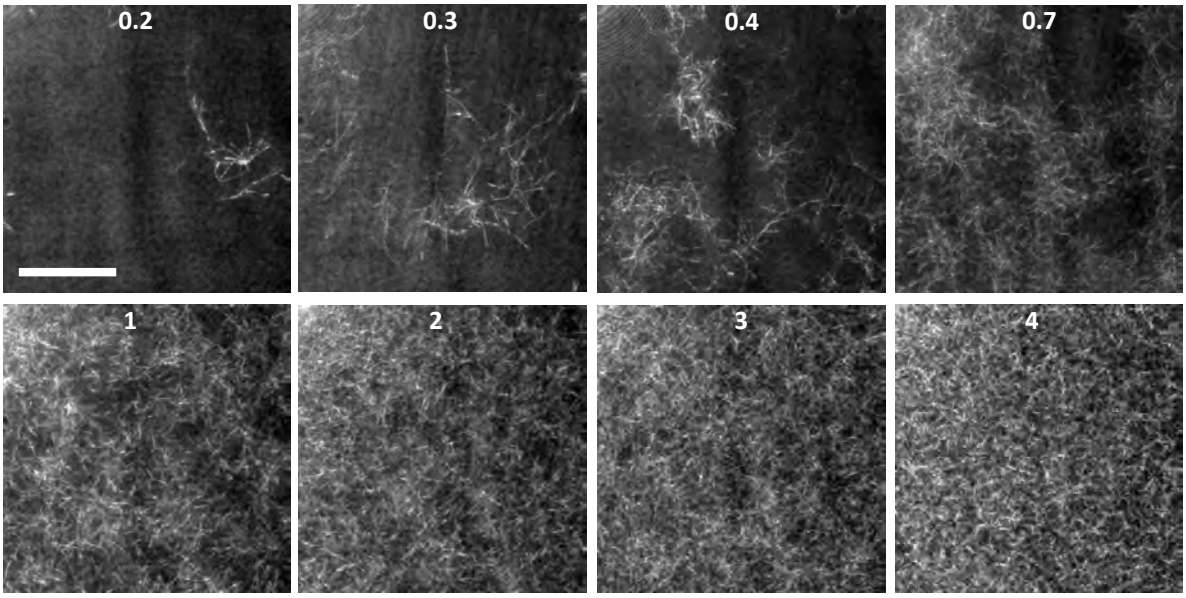

Figure S10: Confocal reflection images of collagen networks formed at 37°C for concentrations ranging from 0.2 to 4 mg/ml (see labels). Scale bar denotes 20 μm for all images. All images are summations over a distance of 20 μm in z with a z-spacing of 0.2 μm. Time lapse images of dilute collagen gels (<0.5 mg/ml) reveal obvious dangling ends. For 0.7 mg/ml and higher, there are no discernible dangling ends and the networks become denser and more uniform with increasing collagen concentration.

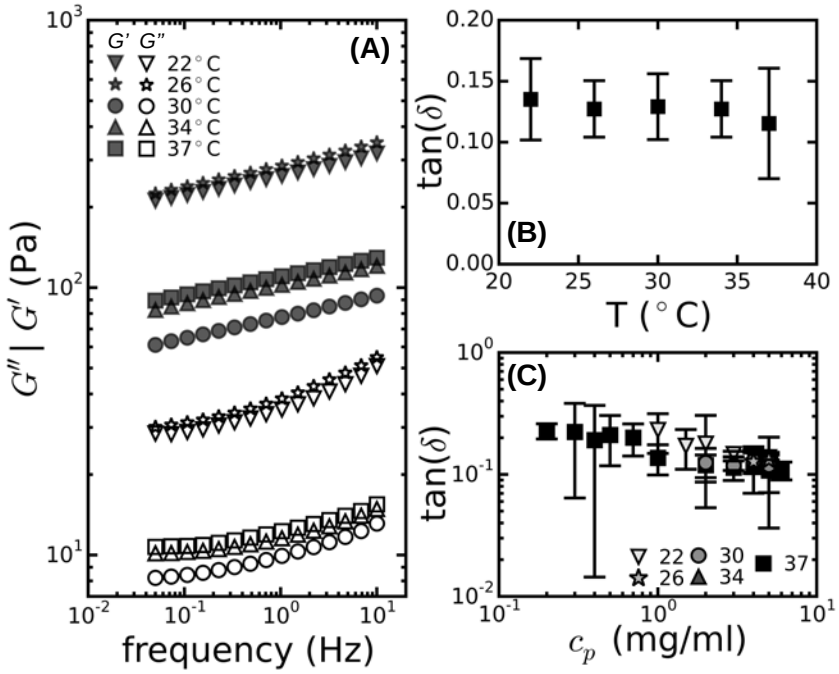

Figure S11: Viscoelastic properties of collagen networks. (A) Frequency dependence of the elastic and viscous shear moduli, G' (closed symbols) and G'' (open symbols), for 4 mg/ml collagen gels polymerized at temperatures of 22°C (triangles down), 26°C (stars), 30°C (circles), 34°C (triangles up) and 37°C (squares). Inset: temperature dependence of the loss tangent (G'/G) at 0.5 Hz. (B) Concentration dependence of the loss tangent, tan(δ), at 22°C (triangles down), 26°C (stars) , 30°C (circles), 34° (triangle up) and 37°C (squares) in increasing shades of gray. Data shown in (A) are representative curves, while data shown in (B) and (C) are averages $\pm$ standard deviation for 3 samples per condition.

6 Supplementary Tables

T (°C)	c_p (mg/ml)	γ_0 (-)	$\langle z \rangle$	$F(z)$	G_0 predicted (Pa)	G_0 measured (Pa)
37	0.7	0.204 ± 0.025	2.77 ± 0.12	0.09 ± 0.017	0.99	1.69 ± 0.43
	1	0.176 ± 0.014	2.91 ± 0.06	0.11 ± 0.01	3.10	4.08 ± 0.93
	2	0.140 ± 0.009	3.07 ± 0.04	0.14 ± 0.007	20.29	27.15 ± 8.22
	3	0.144 ± 0.008	3.05 ± 0.03	0.14 ± 0.006	65.10	65.23 ± 11.2
	4	0.134 ± 0.014	3.10 ± 0.16	0.14 ± 0.014	63.04	147.5 ± 44.0
	5	0.116 ± 0.003	3.18 ± 0.04	0.17 ± 0.004	360.2	295.8 ± 76.0
34	4	0.143 ± 0.005	3.06 ± 0.02	0.13 ± 0.003	97.9	147.9 ± 35.1
30	2	0.052 ± 0.002	3.52 ± 0.01	0.37 ± 0.008	36.4	34.4 ± 11.9
	3	0.025 ± 0.003	3.70 ± 0.02	0.70 ± 0.032	210	162.6 ± 26.1
	4	0.089 ± 0.007	3.31 ± 0.04	0.22 ± 0.013	137.1	89.0 ± 12.9
	5	0.056 ± 0.02	3.5 ± 0.12	0.38 ± 0.118	332.4	339.2 ± 190
26	4	0.046 ± 0.003	3.55 ± 0.01	0.40 ± 0.012	208.6	324.1 ± 32.8

Table S1: Average network connectivity $\langle z \rangle$ of collagen networks inferred from the nonlinear rheology data by comparing measurements of the onset strain for strain-stiffening γ_0 against predictions for disordered 2D-fiber networks (c.f. Figure 4A-B in the main text). The table furthermore compares measurements of the linear elastic modulus G_0 (last column) with predictions calculated with Eq. (1) in the main text using these same $\langle z \rangle$ values as input, together with measurements of the fiber mass-length ratio. Note that the factor $F(z)$ used in the calculations was computed using the prefactor $A = 1.5$ valid for 3D (22). The 2D prefactor would be A = 4.2 (20).

$\langle z \rangle$	L/l_c	f	ϕ	γ_0 (-)	γ_c (-)
3	2.59	0.7	2.2	0.155	0.274
3.12	2.87	0.73	2.1	0.129	0.21
3.2	3.10	0.75	2.1	0.11	0.185
3.36	3.74	0.77	2.1	0.081	0.146
3.56	5.13	0.81	2	0.044	0.082
3.72	7.06	0.83	2	0.022	0.0409
3.81	9.08	0.85	2	0.014	0.025
3.87	10.99	0.89	2	0.0096	0.014

Table S2: Parameters used in 2D simulations of disordered fiber networks with different architectures (as characterized by $\langle z \rangle$ and L/l_c). The critical scaling exponents, f and ϕ, characterize the strain-controlled transition from bend- to stretch-dominated elasticity that takes place at γ_c and determine the proportionality between γ_0 and γ_c.

References

1. Newman, S., M. C. C. Allain, G. Forgacs, and D. Beysens, 1997. Viscosity and Elasticity During Collagen Assembly In Vitro: Relevance to Matrix-Driven Translocation. Biopolymers 41:337–347.
2. Wood, G., and M. Keech, 1960. The Formation of Fibrils from Collagen Solutions. 1. The Effect of Experimental Conditions: Kinetic and Electron-Microscope Studies. Biochemical Journal 75:588–589.
3. Hwang, Y.-J., and J. G. Lyubovitsky, 2011. Collagen hydrogel characterization: multi-scale and multi-modality approach. Analytical Methods 3:529–536.
4. Zhu, J., and L. J. Kaufman, 2014. Collagen I Self-Assembly: Revealing the Developing Structures that Generate Turbidity. Biophys. J. 106:1822–1831.
5. Piechocka, I. K., A. S. van Oosten, R. G. Breuls, and G. H. Koenderink, 2011. Rheology of Heterotypic Collagen Networks. Biomacromolecules 12:2797–2805.
6. Vader, D., A. Kabla, D. Weitz, and L. Mahadevan, 2009. Strain-Induced Alignment in Collagen Gels. PLoS ONE 4:e5902.
7. Carr, M. E., and J. Hermans, 1978. Size and Density of Fibrin Fibers from Turbidity. Macromolecules 11:46–50.
8. Yeromonahos, C., B. Polack, and F. Caton, 2010. Nanostructure of the Fibrin Clot. Biophys. J. 99:2018–2027.
9. Ferri, F., G. R. Calegari, M. Molteni, B. Cardinali, D. Magatti, and M. Rocco, 2015. Size and density of fibers in fibrin and other filamentous networks from turbidimetry: beyond a revisited Carr-Hermans method, accounting for fractality and porosity. Macromolecules 48:5423–5432.
10. Brokaw, J., C. Doillon, R. Hahn, D. Birk, R. Berg, and F. Silver, 1985. Turbidimetry and morphological studies of type I collagen fiber assembly in vitro and the influence of fibronectin. Int. J. Biol. Macromol. 7:135–140.
11. Wess, T., 2005. Collagen fibril form and function. Adv. Protein Chem. 341–374.
12. Baradet, T. C., J. C. Haselgrove, and J. W. Weisel, 1995. Three-Dimensional Reconstruction of Fibrin Clot Networks from Stereoscopic Intermediate Voltage Electron Microscope Images and Analysis of Branching. Biophys. J. 68:1551–1560.
13. Gersh, K. C., C. Nagaswami, and J. W. Weisel, 2009. Fibrin network structure and clot mechanical properties are altered by incorporation of erythrocytes. Thromb. Haemost. 102:1169–1175.
14. de Wild, M., W. Pomp, and G. H. Koenderink, 2013. Thermal Memory in Self-Assembled Collagen Fibril Networks. Biophys. J. 105:200–210.
15. Sharma, A., A. Licup, K. Jansen, R. Rens, M. Sheinman, G. Koenderink, and F. MacKintosh, 2016. Strain-controlled criticality governs the nonlinear mechanics of fibre networks. Nature Physics 12:584–587.
16. Maxwell, J., 1864. On the calculation of the equilibrium and stiffness of frames. Philosophical Magazine 27:294–299.
17. Lindström, S. B., D. A. Vader, A. Kulachenko, and D. A. Weitz, 2010. Biopolymer network geometries: Characterization, regeneration, and elastic properties. PRE 82:051905.
18. Licup, A. J., S. Münster, A. Sharma, M. Sheinman, L. M. Jawerth, B. Fabry, D. A. Weitz, and F. C. MacKintosh, 2015. Stress controls the mechanics of collagen networks. PNAS 112:9573–9578.
19. Broedersz, C. P., X. Mao, T. C. Lubensky, and F. C. MacKintosh, 2011. Criticality and isostaticity in fibre networks. Nature Physics 7:983–988.
20. Licup, A. J., A. Sharma, and F. C. MacKintosh, 2016. Elastic regimes of subisostatic athermal fiber networks. PRE 93:012407.
21. Landau, L., and E. Lifshiftz, editors, 1970. Theory of elasticity. Pergamon Press, Oxford, 2nd edition.
22. Broedersz, C., M. Sheinman, and F. MacKintosh, 2012. Filament-Length-Controlled Elasticity in 3D Fiber Networks. PRL 108:078102.